FOAMING OF WASTE GLASS OF A GLASS POLISHING FACTORY

A Thesis Submitted to
the Graduate School of Engineering and Sciences of
İzmir Institute of Technology
in Partial Fulfillment of the Requirements for the Degree of

MASTER OF SCIENCE

in Materials Science and Engineering

by
Yiğit ATTİLA

July 2012
İZMİR

We approve the thesis of **Yiğit ATTİLA**

Examining Committee Members:

Assoc. Prof. Dr. Alper TAŞDEMİRCİ
Department of Mechanical Engineering
İzmir Institute of Technology

Prof. Dr. Muhsin ÇİFTÇİOĞLU
Department of Chemical Engineering
İzmir Institute of Technology

Assoc. Prof. Dr. Mustafa M. DEMİR
Department of Chemistry
İzmir Institute of Technology

06 July 2012

Assoc. Prof. Dr. Alper TAŞDEMİRCİ
Supervisor, Department of Mechanical Engineering
İzmir Institute of Technology

Prof. Dr. Mustafa GÜDEN
Co-Supervisor, Department of Mechanical Engineering
İzmir Institute of Technology

Assoc. Prof. Dr. Mustafa M. DEMİR
Head of the Department of Materials Science and Engineering

Prof. Dr. R. Tuğrul SENGER
Dean of the Graduate School of Engineering and Sciences

ACKNOWLEDGEMENTS

I would like to express my deep and sincere gratitude to my supervisor Associate Prof. Dr. Alper TAŞDEMİRCİ and my Co-Advisor. Prof. Dr. Mustafa GÜDEN for their instructive comments, encouragement, guidance and support from the beginning to the final stage enabled to me to completely understand the subject.

I gratefully thank to my colleagues, Umut Savacı, Doğuş Zeren, Ali Kara, Kutlay Odacı, Cenk Kılıçaslan, Ali Kıvanç Turan, Levent Yurdaer Aydemir and z-46 crew for their support and help. I also wish to thank my family who deserve a special mention for their endless support and prayers. Also I would like to thank the IYTE-MAM research center staff

A very special thank goes to a very special girl, Ezgi Kaya, her great support, patience and giving motivation during my study and being a part of my life Finally, I would like to thank everyone who helped me during this thesis and I offer an apology that I could not mention personally one by one.

ABSTRACT

FOAMING OF WASTE GLASS OF A GLASS POLISHING FACTORY

The foaming behavior of a glass powder, a residue from a window glass polishing factory in Bursa, was investigated at the temperatures between 700-950°C. As-received glass powder composition, 72.76% SiO_2, 11.18% Na_2O, 11.31% CaO, 1.74% MgO and 1.61% Al_2O_3, was well matched with that of soda lime window glass. The expansion of the glass powder compacts started at a characteristic temperature of 690-700 °C and reached a maximum volumetric expansion values at about 866-877 °C. The maximum volume expansion and foam density varied between 700-772% and 0.378-0.206 g/cm3, respectively. The foaming of the compact at 750 °C yielded only crystalline phase of quartz, as the foaming temperature increased over 750 °C, wollastonite and diopsite crystals formed The compressive strength of the foams ranged between 1.9 and 4 MPa and the thermal conductivity between 0.048-0.079 W/K m. Both collapse and plateau stresses increased with increasing relative density, while heating rate was found to be not affect the collapse and plateau stresses. The foamed glass samples showed the mechanical behavior similar to open cell foams. This was attributed to the thicker cell edges and thinner cell walls leading to higher glass material accumulation on the cell edges. The self-foaming behavior of the studied waste glass powder was attributed to the organic compounds within the boron oil which was used as a coolant in the polishing operations.

ÖZET

CAM PARLATMA FABRİKASINDAN ALINAN ATIK CAM TOZUNUN KÖPÜKLEŞME DAVRANIŞI

Bu çalışmada Bursa'daki bir cam parlatma fabrikasından gelen atık cam tozlarının 700-950 °C arasındaki köpükleşme davranışı incelenmiştir. Gelen cam tozu % 72.76 SiO_2, %11.18 Na_2O, %11.31 CaO, %1.74 MgO ve %1.61 Al_2O_3 içermektedir. Cam tozu kompaktlarının hacimce genleşmesi 690 ve 700 °C aralığında başlamış ve en yüksek hacimce genleşme 866-877 °C aralığında gözlenmiştir. Bu sıcaklıklardaki hacimce genleşme %700-772 olarak elde edilirken, köpük malzemenin yoğunluğu 0.378-0.206 g/cm^3 olmuştur. 750 °C'de gözlenen tek kristal fazı kuvars iken, sıcaklık yükseldikçe vollastonit ve diopsit kristalleri oluşmuştur. Ürünlerin basma mukavemeti 1.9 MPa ve 4 MPa arasında değişirken ısıl iletkenlik değerleri 0.048-0.079 W/m*K arasında gözlenmiştir. Basma mukavemeti ve plato stres değerlerinin yoğunluğun artması ile yükseldiği görülmüştür. Öte yandan ısıtma hızının plato strese bir etkisi gözlenmemiştir. Cam köpük numunelerin mekanik davranışlarının açık hücreli köpük malzemelere benzediği anlaşılmıştır. Son olarak tozun köpükleşme davranışının parlatma esnasında soğutma amaçlı kullanılan bor yağının içindeki organik bileşiklerden kaynaklandığı anlaşılmıştır.

TABLE OF CONTENTS

LIST OF FIGURES

Figure **Page**

LIST OF TABLES

Table **Page**

CHAPTER 1

INTRODUCTION

1. Introduction

Industrial waste recycling is a way of disposing industrial waste. Recycling as matter of concern in the developing countries is not only important for transforming the wastes into useful products in a cost effective way but also important for reserving the natural sources for future generations. Foam glass production based on waste glass is a good example to such efforts. Although, foam glass parts have been commercially available since the 1930's, the interests on the materials are resumed nowadays. This is partly due to the advantages of foam glass over the foams currently used for the similar applications. Foam glass has relatively low thermal conductivity with good mechanical properties, relatively high resistance to chemical attack and fire and low water vapor.

Almost 80% of the recycled glass is not suitable for re-melting in the glass processing factories and needs to be recycled into a cheap and suitable product. Foam glass processing using glass cullet is one way of recycling waste glass. The foam glass processing based on the use of glass powder or ground glass is a well-developed process in which the glass powder is foamed at an elevated temperature in the presence of a blowing agent, carbon or a carbon containing compound and an oxidizing agent. Over the years, various types of foaming agents have been identified including calcium carbonate, graphite, silicon carbide and silicon nitride.

Currently, there are three major foam glass products largely based on waste glass: loose aggregates, blocks and pellets. In this thesis, the foaming behavior of a waste glass powder which is a residue from a sheet or window glass polishing factory in Bursa, was investigated for the processing of foam glass blocks. The powder is currently dumped in a field near the factory. The total amount of the powder is estimated to be 30000 tons. One of the very important properties of the investigated glass powder waste is the self-foaming property, which excludes the addition of blowing agent. The compression mechanical properties and thermal conductivities of the prepared foam were also determined.

The content of the thesis is as follows: Chapter II summarizes the foam glass production current status with a literature survey. Experimental set-up, chemical characterization, processing and mechanical testing are explained in detail in Chapter III. The results are given in Chapter IV. Chapter V and Chapter VI are the discussions and conclusions, respectively.

CHAPTER 2

FOAM GLASS: CURRENT STATUS

2.1. Glass Types and Recycling

Container glass is a general name, representing bottles and jars. This is one of the most widely used glass type. The glass bottles production in Japan for example was reported to be about 1.98 million tons in 1998 and 74% of the container glass production was used as waste glass, cullet [1]. In UK, the cullet is estimated to reach about 0.5 million tons per year [2]. *Flat glass*, also called *sheet glass* or *plane glass*, is produced in plane form and widely utilized in windows and in the similar applications. It is the second largest sector of glass manufacture and used for longer terms. *Fiber glass*, long and short fibers, are used to manufacture glass fiber reinforced plastics (composites) and cements. The reutilization of glass fiber is very difficult since it is mixed with a polymeric resin. *Domestic glass* includes ornaments and *special glass* such as the Cathode Ray Tubes (CRTs) used in the televisions and medical and other specialist equipment.

The recycling glass market is largely based on the container glass. The use of or re-melting of cullet for glass processing reduces the energy consumption by 25% compared to glass processing using raw materials. One of the biggest problems in reusing glass cullet in the manufacturing new glass products is the variable color of the cullet collected.

Figure 2.1 shows the steps of container glass recycling [3]. The recycling process starts with removing the ferrous metal items by means of the magnets. Other contaminants are usually removed manually. Next, the cullet is crushed and then sieved into different sizes. The light materials are separated by vacuum hoods and the opaque materials are removed using a high pressure air jet. Finally, the recycled cullet is melted in furnaces to make new bottles and jars. According to UK Environment Agency report, about 670,000-770,000 tons of waste flat glass are generated every year in UK; only 210,000 tons of it are recycled, while the rest goes to landfill [4]. Another study reports that about 900,000 tons of waste glass are generated each year in EU [5]. The glass

bottles production in Japan was about 1.98 million tons in 1998 and 74% of the production was used as cullet [1]. Another study reports that only 20% of the waste glass are collected and returned to glass factories for re-melting [6]. The rest of the waste glass is not suitable for the glass production and needs to be recycled into a cheap and suitable product. Foam glass processing using glass cullet is one way of recycling waste glass. For example, the foam glass production in Russia using cullet is reported to resume in the near future [7].

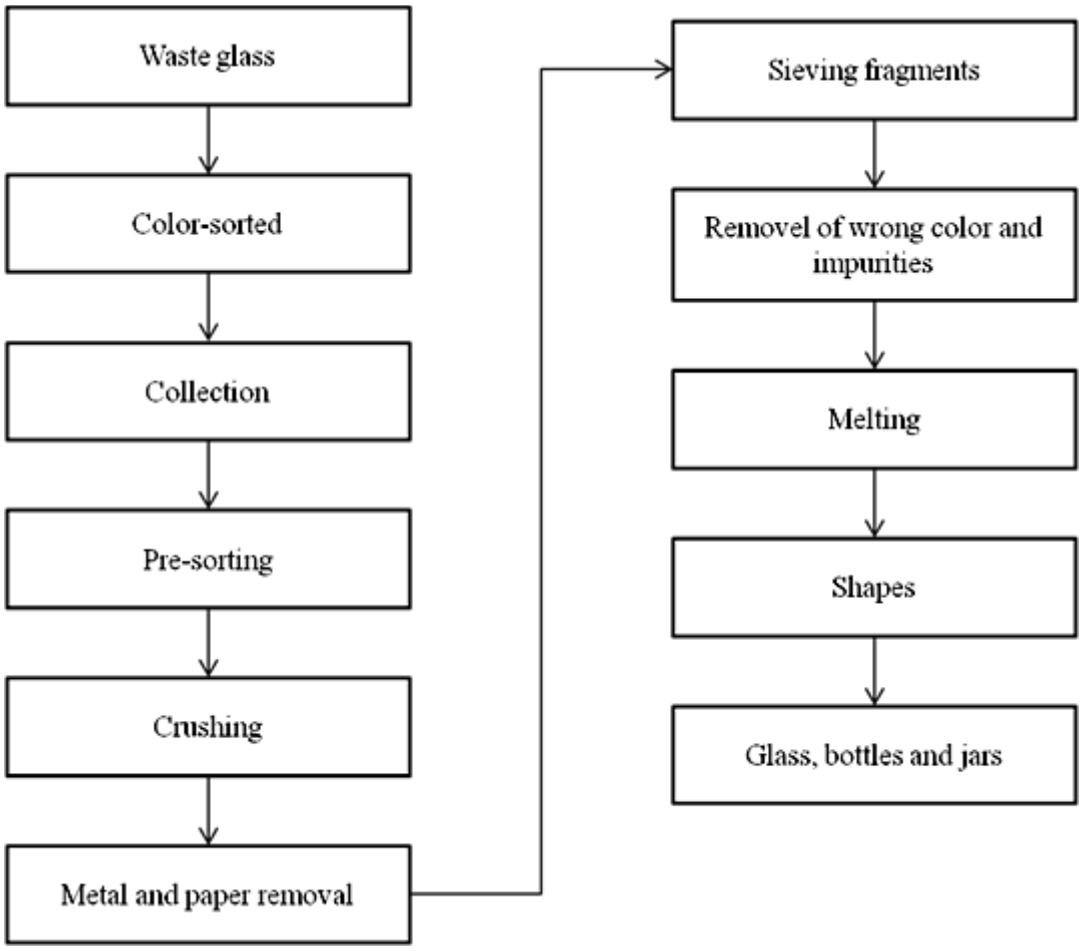

Figure 2.1. Waste container glass recycling process steps.[3]

The compositions of glass cullet suitable for glass foam processing in different countries are tabulated in Table 2.1. The SiO_2 contents of the cullet in countries vary between 67 and 72%, Al_2O_3 between 1 and 6%, CaO between 7 and 11%, MgO between 1 and 7% and Na_2O between 14 and 15%.

Table 2.1. The composition of the container and sheet glass cullet in different countries[8].

	Mass Content								
Country	**SiO_2**	**Al_2O_3**	**Fe_2O_3**	**CaO**	**MgO**	**Na_2O**	**K_2O**	**SO_3**	**MnO**
USA	71.36	0.79	0.12	8.89	0.32	15.38	0.62	0.51	-
Holland	70.92	2.26	0.27	11.41	1.50	12.78	1.04	-	-
Scotland	70.18	2.59	1.25	9.30	0.86	14.07	0.68	0.26	0.13
France	70.40	1.80	-	9.60	1.20	15.00	0.20	-	-
Japan	73.30	2.11	0.10	7.43	0.48	17.50	0.82	-	-
Czech Republic	73.80	0.27	0.03	4.41	3.10	18.06		0.40	0.77
Poland	72.75	1.38	0.06	8.75	0.24	14.35	1.72	0.55	-
Hungary	73.23	2.17	0.30	5.58	2.13	16.15	1.00	0.45	-
	73.41	1.79	0.52	7.23	2.31	14.07	0.38	-	0.03
	71.47	1.39	0.06	7.50	4.36	14.07	0.30	-	-
	69.80	2.72	0.68	6.77	3.37	14.07	-	0.35	0.20
Yugoslavia	70.01	1.99	0.86	7.38	3.23	14.06	0.43	-	0.10
Russia	67.15	6.28	2.89	7.62	0.63	13.95	1.03	-	-
Germany	69.90	1.15	1.29	10.47	1.04	15.01	0.37	0.53	-
Belarus	72.07	2.05	0.42	6.60	4.00	14.86	-	-	-

2.2. Foaming Glass Cullet

Foam glass processing is currently based largely on powder method in which the mixture of glass powder with a blowing agent or gas-forming agent which releases a gaseous product upon heating is heated to an elevated temperature above the melting point of the glass. The ground glass was mixed with a blowing agent, carbon or a carbon containing compound and an oxidizing agent for example $CaSO_4$ or MnO_2. The heating the mixture to the melting temperature lead to the sintering of the glass powder and later foaming the mixture by the evolution of the gases such as CO, CO_2, HS_2, N_2 and etc. The use of a cheaper blowing agent $CaCO_3$ was developed and patented later in 1944 [9]. The use of water as a gasifying agent similar to natural pearlite in foaming waste glass was also developed [10].

The foam glass processing is generally characterized by three stages as depicted in Figure 2.2. In stage I, the glass powder with blowing agent is heated up to foaming temperature within a certain duration of time. In stage II the foaming takes place and in the final stage the foamed glass is cooled and annealed (point A). It was reported that the combustion of carbon contributed only 29% of the heat required for foaming and 20 – 40% of the initial carbon was combusted with gases being released [11]. The use of liquid hydrocarbons foaming agents were recommended to retard the effect on the combustion reaction rate.

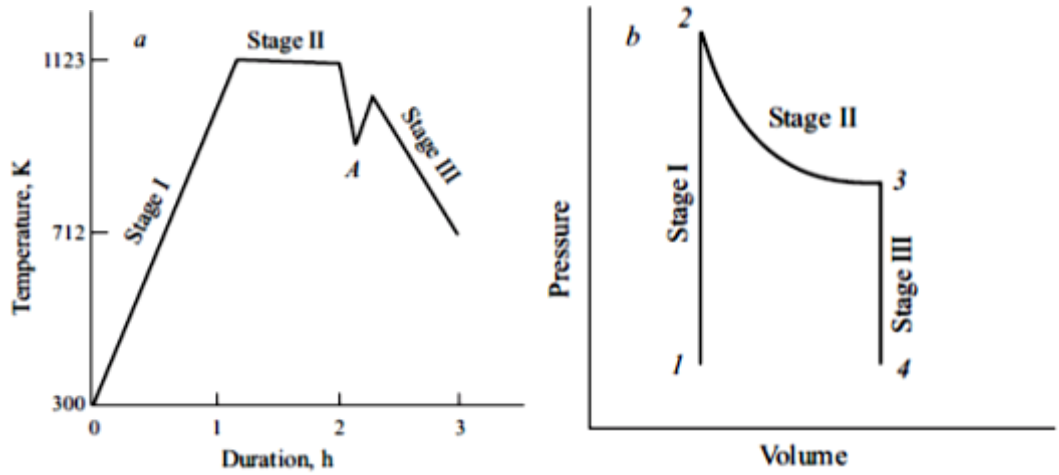

Figure 2.2. (a) The temperature–time (b) pressure time graph of glass powder foaming process [11].

The foaming of fused glass or vitreous silica pellets with entrapped blowing agent was developed in 1970s [9]. In this method, the silica was ground and mixed with a blowing agent (0.1% lampblack). Then, the mixture was fused in a furnace under pressure. The crushed melts were finally foamed in a furnace. Using this method various glass types including Pyrex were successfully foamed [9]. It was also shown that silicon carbide (SiC) and silicon nitride (Si_3N_4) were very effective in foaming borosilicate glasses over a wide range of temperatures [12]. The addition of alumina-containing materials was further shown in the same study to inhibit the crystallization tendency of the glass powders to cristobalite.

The blowing agents are divided in two groups [13]: 1) *neutralizers* and 2) *redox* agents. In the first group, the blowing agent dissociates to give a gaseous product, for example dolomite ($CaMg(CO_3)_2$) upon heating gives $CaCO_3$ and CO_2 through the following reaction:

$$CaMg(CO_3)_2 \rightarrow CaCO_3 + MgO + CO_2 \quad (2.1)$$

and

$$CaCO_3 \rightarrow CaO + CO_2 \quad (2.2)$$

The first reaction occurs at 800 ^oC and the second at about 890 ^oC [14]. When calcium carbide was used as a blowing agent along the second reaction takes place. In foaming with redox agents such as coal, coke, graphite, lampblack, silicon carbide, the gas emission (oxygen and sulfuric anhydride) is due to the oxidation of the gas forming agents by the dissolved gases in glass melt and the oxygen gas in the foaming environment,

$$C + O_2 \rightarrow CO_2 \quad (2.3)$$

and

$$2C + O_2 \rightarrow 2CO \quad (2.4)$$

Typical reaction leading to the formation of pores by gas evolution when SiC, Si_3N_4 and aluminum nitride (AlN) used as blowing agent are sequentially,

$$SiC + 2O_2 \rightarrow SiO_2 + CO_2 \quad (2.5)$$

$$Si_3N_4 + 3O_2 \rightarrow 3SiO_2 + 2N_2 \quad (2.6)$$

and

$$4AlN + 3O_2 \rightarrow 2Al_2O_3 + 2N_2 \quad (2.7)$$

When an oxidation agent is used such as MnO_2 following reactions take place in addition to above reactions, the following reactions take place,

$$2SiC+3MnO_2 \rightarrow 2SiO_2+3Mn+2CO \quad (2.8)$$

$$Si_3N_4+6MnO_2 \rightarrow 3SiO_2+6MnO+2N_2 \quad (2.9)$$

The alkali treatment of glass powder was reported to result in formation of an intermediate layer on the surfaces of glass which reduces the melting point by 50-100^oC [6].

The foaming of different types of wastes and cheaper blowing agents were previously investigated. The SiC-based glass articles polishing wastes were used as foaming agent in the foaming of soda-lime glass [15]. In an another study, waste soda-lime glass powder mixed with the waste from the glass fiber manufacturing was foamed using SiC as blowing agent [16]. The foaming of glass cullet with the addition of 20 wt% fly ash using marble cutting polishing plant sludge, mainly calcite and dolomite [5] and SiC [5] as blowing agent were investigated. It was shown that the increasing the amount of blowing agent tended to enhance the crystallization of foam glass and limited the melt glass powder expansion by increasing the viscosity. The foaming was performed between 750 and 950 ^oC using marble sludge and dolomite as blowing agent and 900 and 950 ^oC using SiC as blowing agent. The effect of heating rate on the cell size and expansion of soda lime foam glass were investigated [17]. Lower heating rates resulted in lower expansions due to the escaped gases.

2.3. Foaming Dismantled Cathode Ray Tubes

There are two type of CRTs; monochromic and color. The parts of typical color CRTs are shown in Figure 2.3 and consist of three kinds of glasses; *funnel glass*, *panel glass* (screen) and very thin layers of *faceplate*. The chemical compositions of CRT glasses are further tabulated in Table 2.2 [18]. The panel glass is a barium-strontium glass containing relatively expensive oxides, BaO and SrO. The funnel glass contains high concentrations of PbO (22 wt%). About 2/3 of the total weight of CRT is panel glass [19].

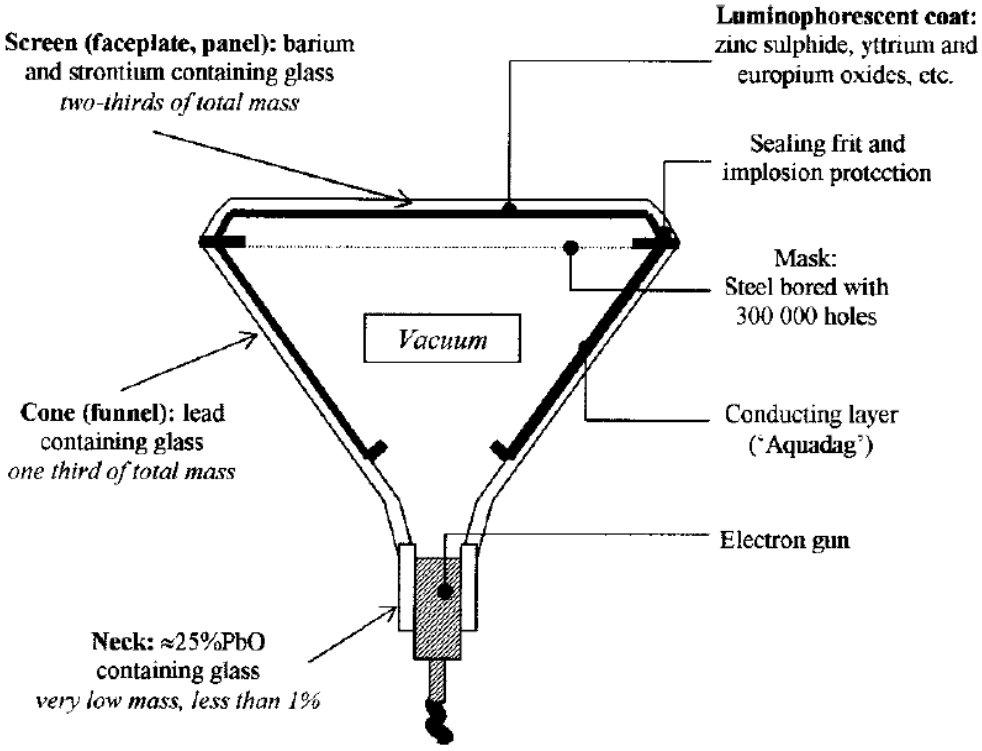

Figure 2.3. The parts of CRTs [18].

Table 2.2 CRT glass compositions in wt%[18].

Compound	Black and White Glass		Color Screen Glass		Color Funnel Glass	
	Range	Standard Content	Range	Standard Content	Range	Standard Content
Network Formers						
SiO_2	64-66	65	60-63	62	52-56	52
Sb_2O_3	0.3-0.6	0.45	0.25-0.50	0.35	0.1-0.3	0.25
ZrO_2	0-0.5	0.25	0-2.5	1.5	-	-
As_2O_3	0-0.3	0.25	0-0.2	0.02	0-0.1	0.01
Intermediaries						
Al_2O_3	3-5	3	2-3.5	2.2	3.5-5	4
PbO	2.8-4.4	4	0-3	-	19-23	22
ZnO	0-0.1	0.05	0.4-0.6	0.5	0-0.1	0.05
TiO_2	0.1-0.2	0.15	0.4-0.6	0.5	0-0.1	0.05
Network Modifiers						
Na_2O	6.5-8	7	7.8-9	8	6-8	6.8
K_2O	6-7.5	7	6-7.5	7.5	7.5-8.5	7.8
Li_2O	0-0.6	0.3	0-0.5	0.2	0-0.1	-
CaO	0-1	0.5	0-2	0.5	2-4	3.8
MgO	-		0-1	0.2	1.2-2	1.8
Fe_2O_3	0.05-0.2	0.12	0.07-0.12	0.08	0.05-0.07	0.06
SrO	0-2	1	6-10	8.5	0-1	0.5
BaO	9-12	11	9-11	10	0-2	1
CeO_2	0.1-0.2	0.18	0.2-0.3	0.25	-	

The dismantled CRTs cannot be used directly in glass component processing as they contain heavy metal oxides. The CRTs are generally disposed into licensed land fields or they are reutilized in the processing CRTs. In recent years, there has been growing interest and investigations on the recycling of CRT glass through glass foam processing [18-22]. Bernardo et. al. [23] investigated the foaming behavior CRT panel glass using a neutralizer blowing agent, $CaCO_3$. The foaming experiments were performed at constant foaming temperature of 725 ^oC; at various heating rates (5, 20 °C/min), holding times (5 to 30 min) and concentrations of blowing agent (3, 5 and 7%). The prepared foam densities ranged between 190 and 350 kg m^{-3}, crushing strength around 1 MPa and thermal conductivity between 0.06 and 0.07 W m^{-1} K^{-1}. Mear et. al. [18, 20] investigated foaming behavior of CRT funnel glasses using redox blowing agents of 4% SiC and 5% TiN. The foaming was performed between 800 and 900 ^oC. The reaction between lead oxide and reducing agent yielded a gaseous phase of

CO_2 for SiC and N_2 for TiN and metal lead. Metallic lead was shown microscopically to form on the pore surfaces (white spherical particles in Figure 2.4). Following reactions were presumed to occur during foaming

$$2PbO+TiN \rightarrow 2Pb+TiO_2+1/2N_2 \quad (2.10)$$

and[22]

$$4PbO+SiC \rightarrow Pb+SiO_2+CO_2 \quad (2.11)$$

$$2O_2+3Pb \rightarrow Pb_3O_4 \quad (2.12)$$

TiO_2 and SiO_2 were found in the vitrous phase of foam cells as depicted in Figure 2.4.

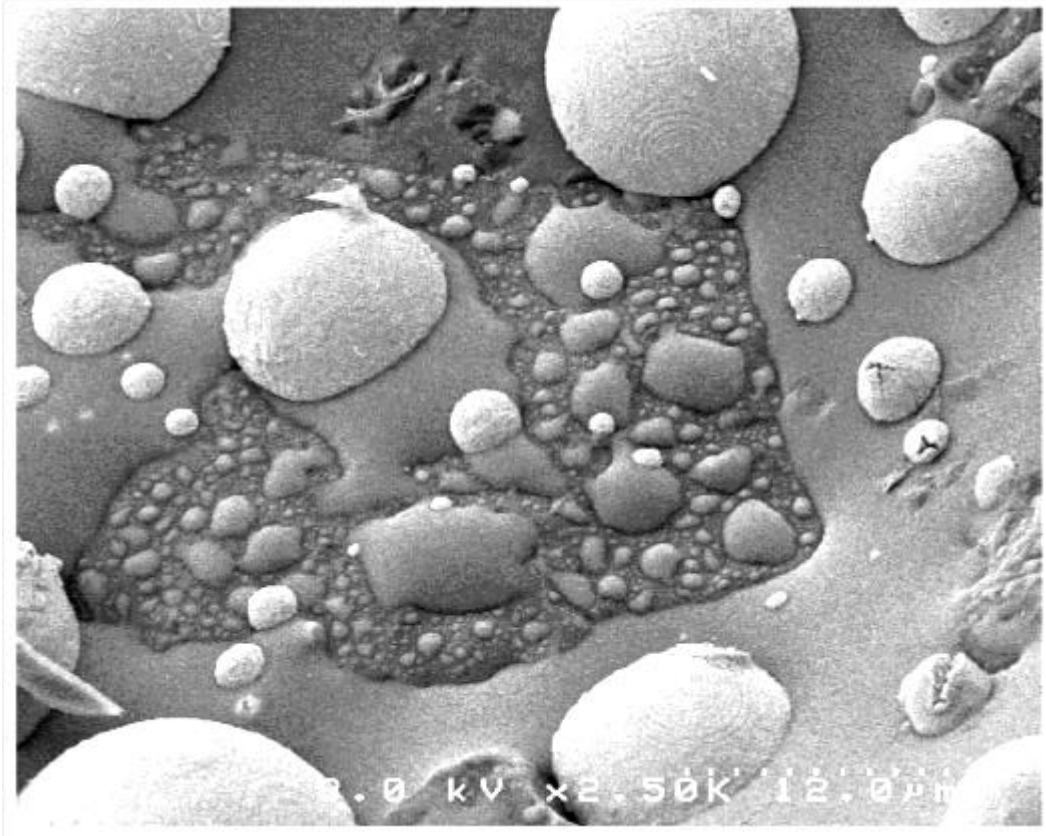

Figure 2.4. SEM picture of metallic lead and vitreous phase [18]

Guo et. al. [22] investigated the foaming behavior of CRT funnel glass powder at a foaming temperature of 850 ^oC using SiC as blowing agent. XRD analysis showed

the presence of Pb, Pb_3O_4, and $Al_6Si_2O_{13}$ microcrystals, which was reported to contribute to the relatively high strength of foam glass samples prepared.

Matamoros et. al. [24] investigated the feasibility of foaming CRT panel glasses through hydrothermal hot-pressing. The glass powder compacts for foaming experiments were hot pressed at 200 ^oC under a pressure of 20 MPa with 5 and 10 wt% of water content. The water was found between the particles and the increase of temperature promoted the chemical reaction between water and glass particles, leading to formation of glass viscous phase. The microstructure of the glass compacts prepared constituted by two major phases: the remaining original glass particles (white particles) and a continuous phase (grey area) that covers the glass particles, which corresponds to the new glass phase (Figure 2.5). The foaming was performed over a temperature range of 650–850 ^oC for 1 h. A preferential crystallization of three major phases, quartz (SiO_2), barium silicate ($BaSiO_3$), potassium silicate (K_2SiO_3) and barium–potassium silicate ($K_2Ba_3Si_8O_2$) was determined during the foaming.

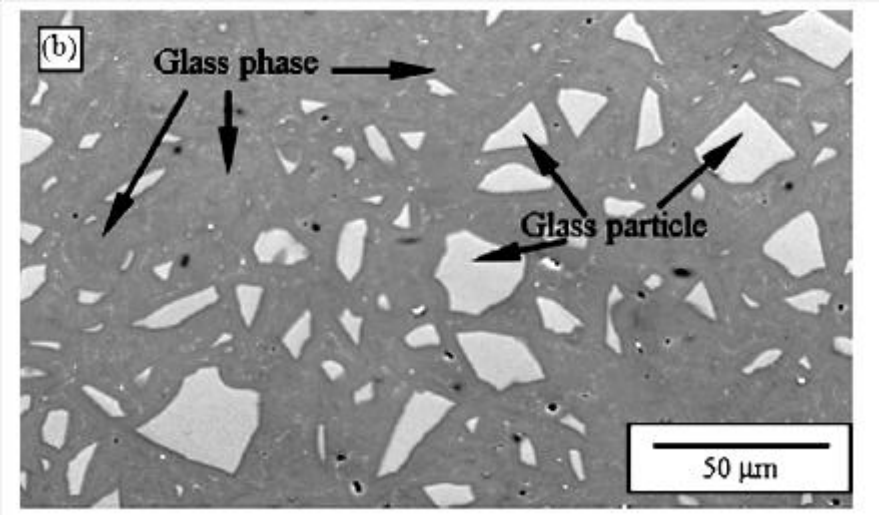

Figure 2.5. SEM micrographs of the CRT glass compacts prepared at 200 ^oC, with a particle size with water contents of 10 wt% [24].

A novel and effective process for the recovery of lead in dismantled funnel CRT glass was also proposed [25]. The technique was based on pyro-vacuum processing of crushed funnel glass powder with carbon. The optimum temperature, pressure, carbon percentage addition and holding time for lead recovery were determined as 1000 ^oC, 1000 Pa, 5% and 4 h, respectively. The maximum lead recovery rate was 98.6%. In the

funnel glass was firstly detached and changed to PbO, then reduced and evaporated, and was recovered in the form of pure metal with a purity of 99.3%[25].

2.4. Foam Glass Production

2.4.1. Continuous Foam Sheet Processing

Continuous foam sheet processing steps using cullet are depicted in Figure 2.6. The first step comprise processing of 75-150 μm glass powder from pre-crushed waste glass (5-20 mm) through using a hammer mill (down to 1 to 2 mm) then a rod or ball mill (down to 100 μm). The powder is then stored before passed to the foaming stage. The glass powder feed stock is then mixed with a foaming agent with the particle size of 75-150 μm. Depending on the final cell structure, dry or wet feedstock can be prepared. Wet feedstock usually ends up with open cell structure. The foaming is usually performed in a tunnel furnace between 700 and 900°C. The feedstock is continuously fed into the furnace through moving belts. The continuous foam furnace consists of three regions: pre heat zone, heating zone and cooling zone as depicted in Figure 2.7. In the cooling zone the foam glass is annealed to reduce the extent of internal stresses. The foam glass with 2 m wide and a thickness of up to 10 cm is then cut into sheets. To produce loosely aggregates, foam slabs can be broken into pieces. In batch type processing, the feed stock is placed inside the molds and the feedstock is heated with mold. Typical picture of foam sheet panel is shown in Figure 2.8. Since the panel is exposed to cutting operations the surface of the panel is open. The foam panel foaming in mold usually has a dense glass layer on the surface.

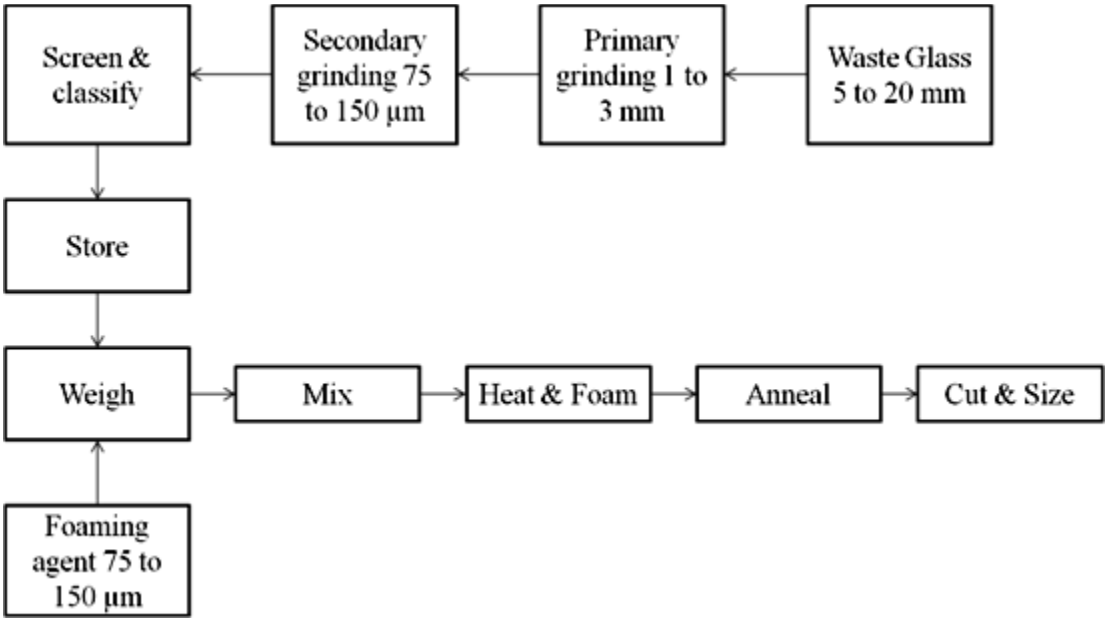

Figure 2.6. Continuous foam sheet processing steps using cullet [3].

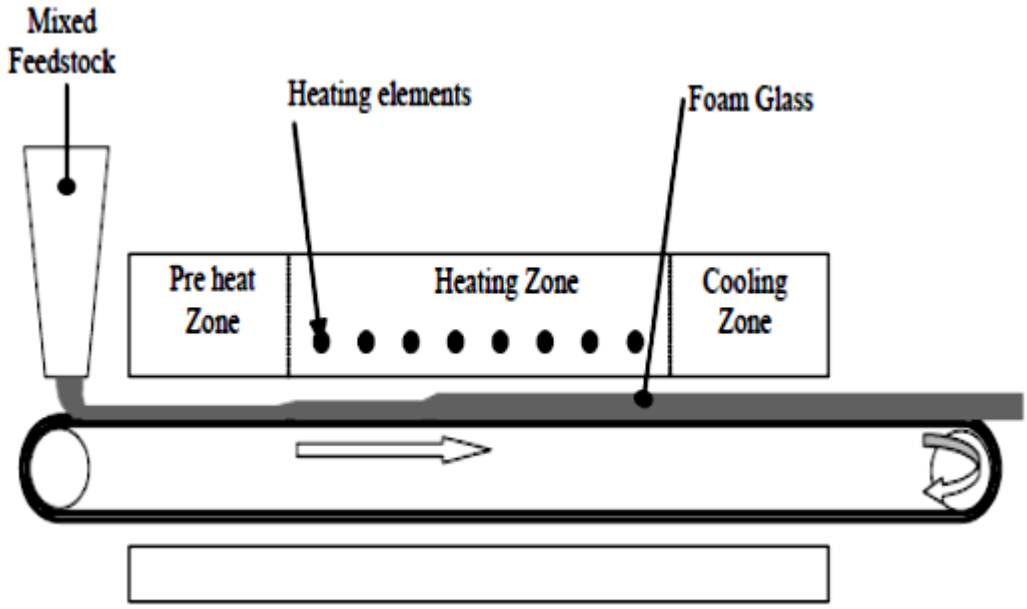

Figure 2.7. The continuous foam furnace with pre-heat zone, heating zone and cooling zone [3].

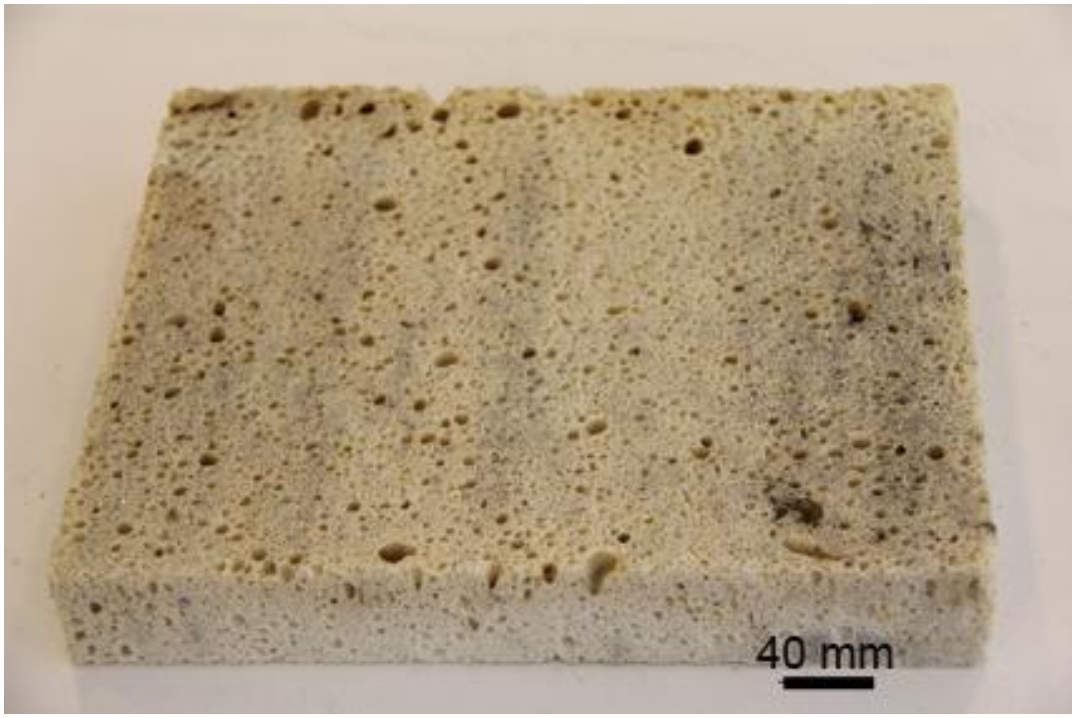

Figure 2.8. Foam glass panel.

2.4.2. Glass Pellet Processing

In the foam glass pellets processing the first step is to prepare glass powder foam agent pellets in a pelletizer (Figure 2.9). The pellet is then fed into a rotary furnace where the heating action drives the foam reaction to take place. The foamed pellets are also annealed and cooled in the same rotary furnace. The size of the pellets processed ranges between 0.5 to 5 mm. Figures 2.10 and 2.11 show the pictures of 500 μm and 5-12 mm foam glass pellets.

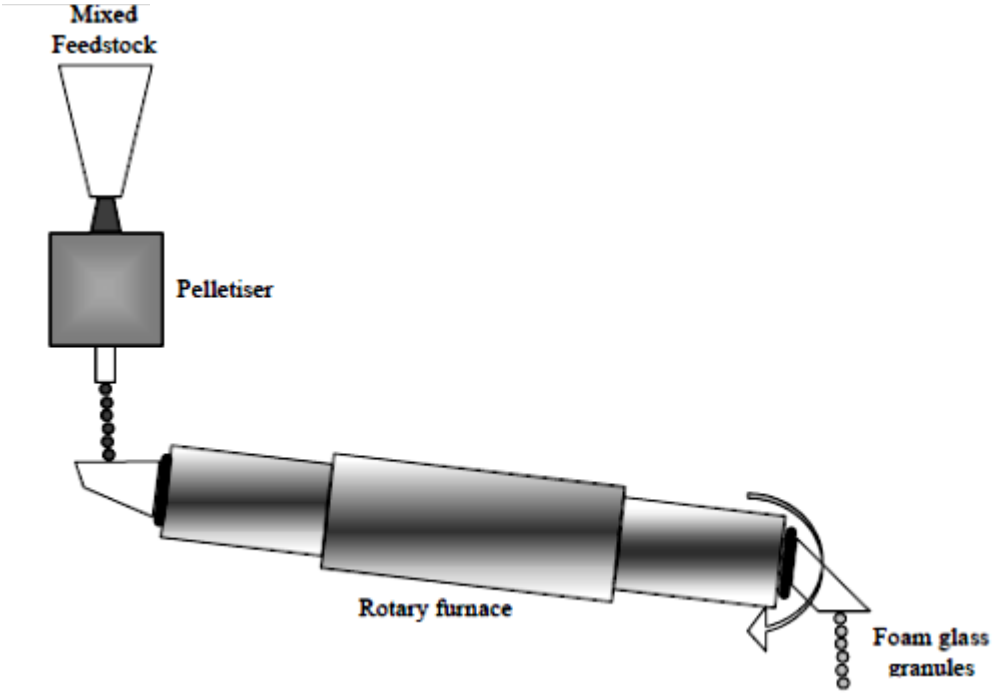

Figure 2.9. Foam glass pellets processing, pelletizer and rotary furnace [3].

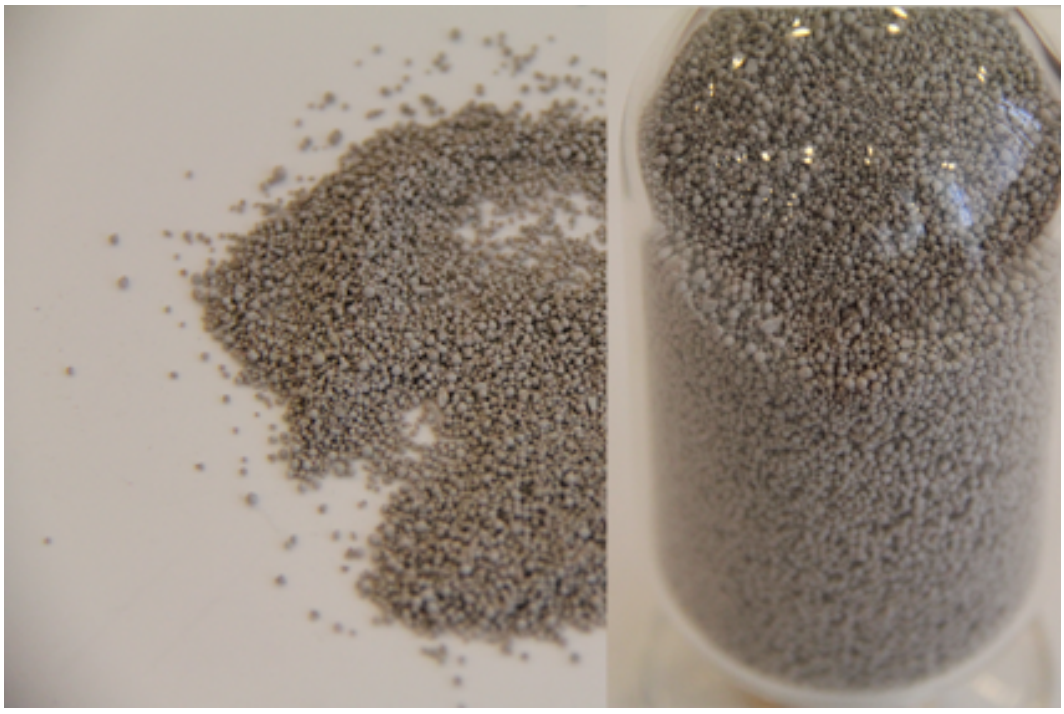

Figure 2.10. Foam glass pellets in 500 μm diameter.

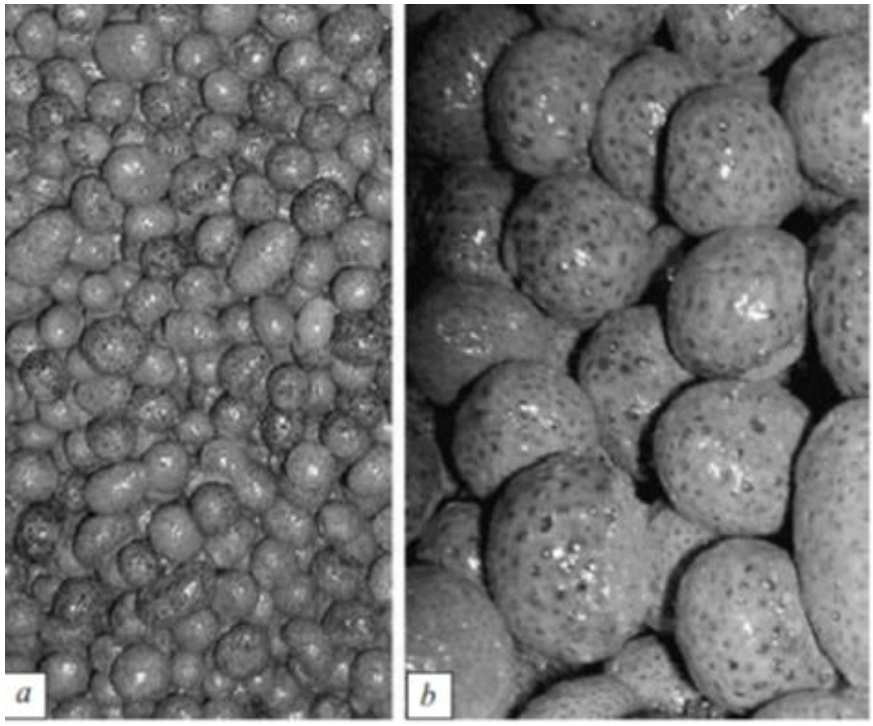

Figure 2.11. Foam glass granules (a) 5-7 mm and (b) 12 mm in diameter [26].

2.5. Properties of Foam Glass

The properties of commercially produced foam glass were previously reported [3] and shown in Table 2.3. The density of commercially available foam glass blocks range between 105- 165 kg m^{-3}. The denser glass powder briquettes were reported to yield lower final foam glass densities [10].

The type of blowing agent either *neutralizers* or *redox* determine the structure and water absorption of foam glass. The water absorption in foams processed using neutralizer blowing agent is as high as 50-70% as the pores are open, while in foams processed using redox gas-forming blowing agent the water absorption ranges between 10-15% [13].

Table 2.3. The properties of commercial foam glass products [3].

Properties	Pittsburgh Corning	Pittsburgh Corning	Cell-u-Foam	Misapor	Millcell	Liaver	Liaver	Geofil Bubles
	Wallboard Block	Foamglass F Block	Ultra-Cuf 1031 Block	Loose aggregate 10 to 50mm	Loose aggregate	Reapor sound insulation	Glass Granules 2 to 4mm	Glass Granules 2 to 25mm
Specific Heat	0.84 kj/kg.K	0.84 kj/kg.K	0.83 kj/kg.K					
Thermal Diffusivity	4.4 x 10^{-7} m^2/s at 0°C	3.5 x 10^{-7} m^2/s at 0°C	4.9 x 10^{-7} m^2/s at 0°C					
Product density	105 kg/m^3	165 kg/m^3	128 kg/m^3	225 kg/m^3	100 to 300 kg/m^3	290 kg/m^3	300 to 500 kg/m^3	450 to 1850 kg/m^3
Bulk Density						190 kg/m^3		250 to 1100 kg/m^3
Porosity				10^6/cm^3		85-86 %		14-50 v%
Water absorption	0	0	0			50-60 m%		0,1-55 m%
Hygroscopicity	0	0	0	0				
Permeability	0	0	0	0				
Capillarity	0	0	0					
Surface water adhesion				70 l/m^3				
Fire	Non-combustible	Non-combustible	Non-combustible	V1 (DIN A1)				Non-Combustible
Toxic fumes	None	None	None	None				None
Dimensional stability	Perfect	Perfect	Perfect					Perfect
Sound transmission loss at normal frequency	28 db/100 mm	28 db/100 mm	28 db/100 mm				> 0.6 (DIN 52215)	42 db/120 mm

The collapse stress of the glass foam is determined with following equation,

$$\sigma_f = \sigma_{bend}[C\sigma\phi\rho_{rel}^{3/2} + (1-\phi)\rho_{rel}] \quad (2.13)$$

where, σ_{bend} is the bending strength of the glass, C is a constant (0.2), ρ_{rel} is the relative density of the foam and ϕ is the volume fraction of the solids contained on the plateau borders. The first term in Eqn. 2.15 is due to bending and the second is due to membrane stretching. Eqn. 2.15 predicts the collapse stress values of open-cell foam when ϕ equals to 1, and the collapse stresses of closed cell foam when ϕ value equals to 0. The values of ϕ can be approximated using the following relation developed for the closed cell tetrakaidecahedral foam.

$$\phi = 1 - \frac{3t(l-2w_p)^2 + 6t\sqrt{3}(l-(2/\sqrt{3})w_p)^2}{11.31l^3\rho_{rel}} \quad (2.14)$$

where l, w_p, and t are the cell wall length, plateau border thickness and cell wall thickness, respectively. The compressive strength of foam glasses are shown in Figures 2.12(a) and (b) as function density. The data in Figure 2.12(a) and (b) are taken from the literature. Until about 500 kg m^{-3}, the compressive stress is up to 4 MPa. Since glass is a brittle material, the fracture of glass is accompanied by elastic deformations. The foam glass show a brittle compression behavior and the microstructure observations revealed the presence of smaller pores on the cell walls as shown in Figure 2.13 [27]. Microscopic studies further showed that the amount of pores on walls decreased with increasing the addition alkali earth aluminosilicate glass powder.

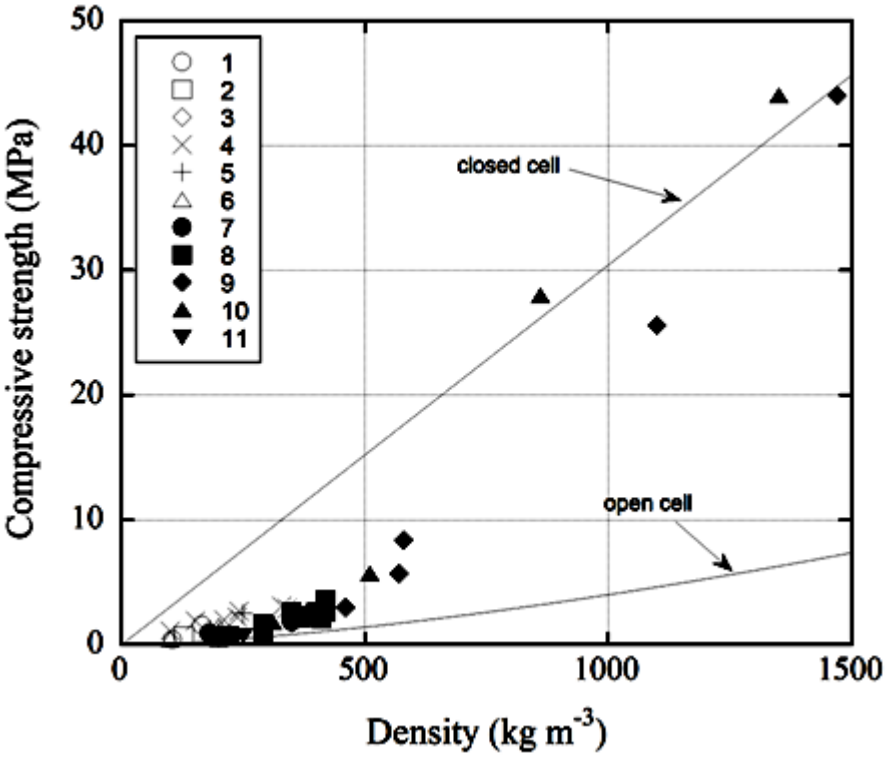

(a)

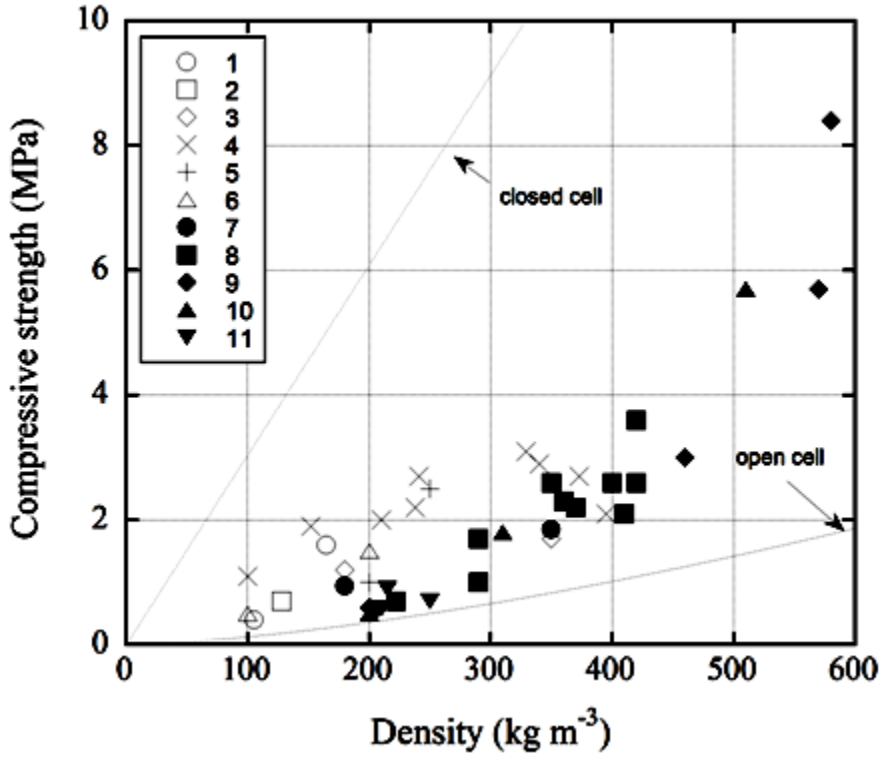

(b)

Figure 2.12. Compressive strength of foam glass (a) and (b).1-[4], 2-[4], 3-[2], 4-[28], 5 -[29], 6-[30],7-[5],8-[16], 9-[31],10- [32], 11-[33]

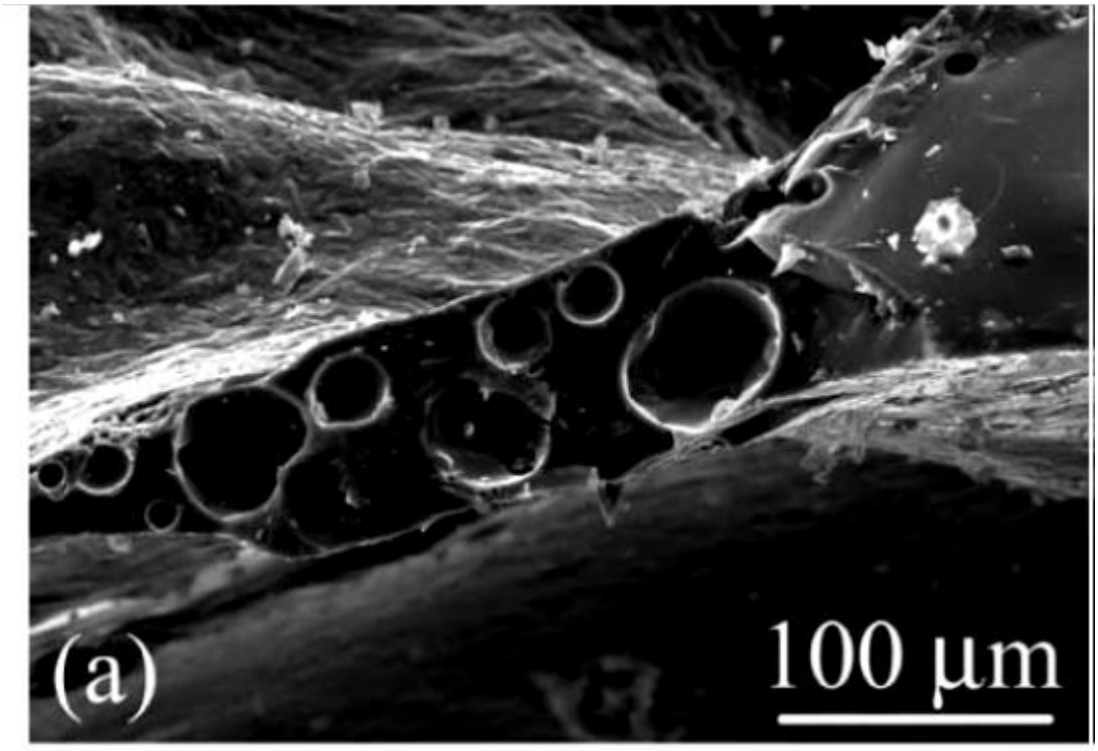

Figure 2.13. The fracture surface of a cell wall in foam glass [27].

The thermal conductivity of foamed glass cannot be higher than about 90% of the volume is occupied by gas and it ranges between 0.05-0.07 W m^{-1} K^{-1} [9]. The thermal conductivity of foam glass as function of density is shown in Figures 2.14(a) and (b). As the density increases the conductivity increases. For the foam densities ranging between 100 and 200 kg m^{-3}, the conductivity range between 0.04 and 0.05 W m^{-1} K^{-1}.

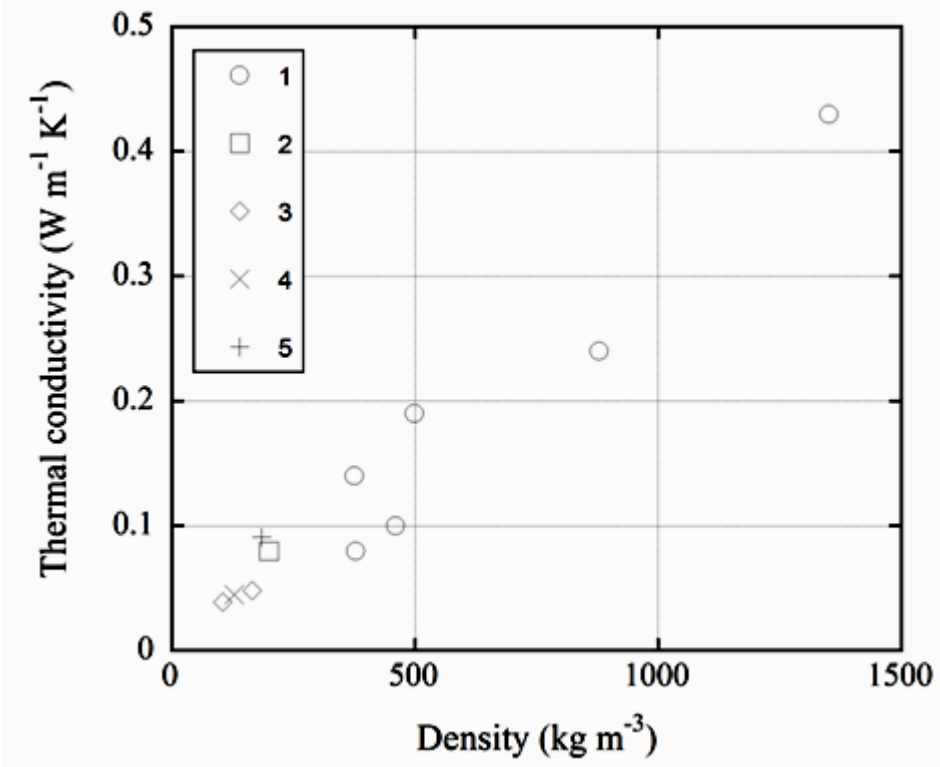

(a)

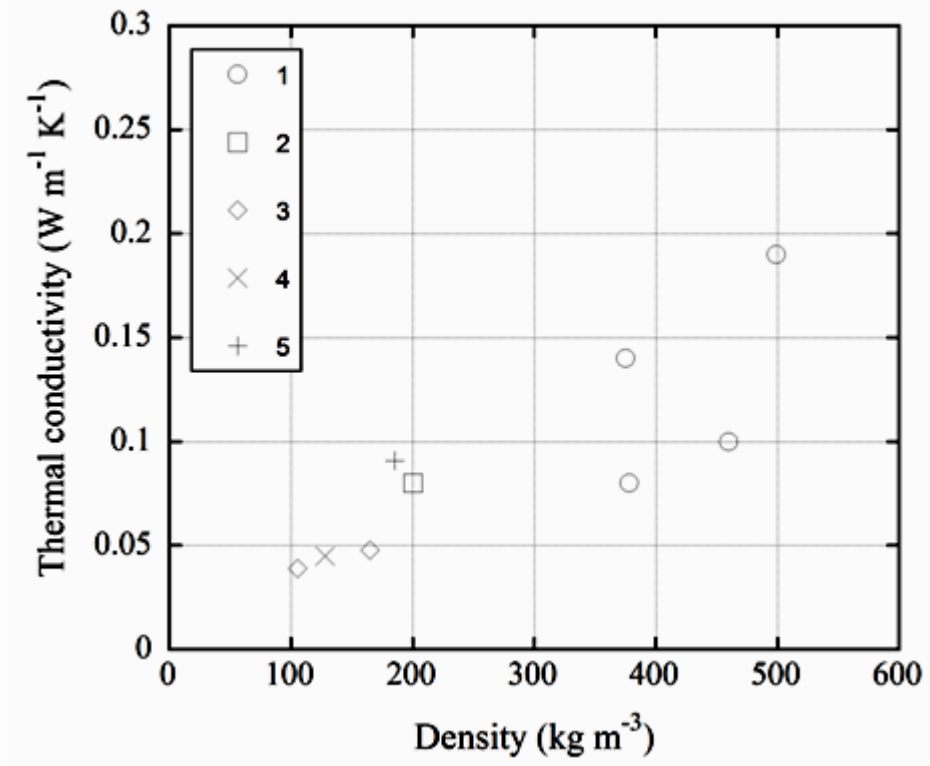

(b)

Figure 2.14. Thermal conductivity of foam glass (a) and (b) 1-[21] , 2-[29] 3-[4], 4-[4], 5-[8].

2.6. Applications

Foam glass with low thermal conductivity surpasses many heat-shielding materials in a number of properties. Foam glass is resistant to water, has relatively high mechanical strength, is incombustible, and satisfies stringent sanitary-hygienic requirements, since it is biologically resistant does not putrefy or get moldy. The relatively high mechanical strength of foam glass facilitates installation, and its biological and chemical resistance ensures constancy of its thermal conductivity values with time. Foam glass is primarily characterized by density.

The use of foamed waste glass as construction material has been proposed recently. Foam glass can be used as light weight filler material for restoration of failed slopes due to rainfall (higher rate of drainage) (see Figure 2.15(a)) (2) subgrade improvement material (mixed with quick lime and used as soft subgrade soil under the pavement (3) improvement material for soft clay, (4) light weight aggregate materials in concrete and (5) water folding material for greening (good water folding material) [1].

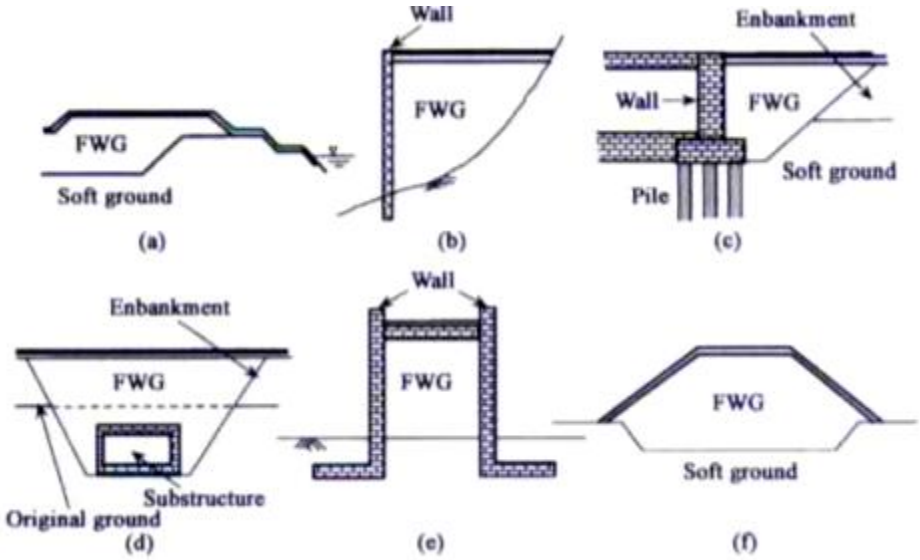

Figure 2.15. Examples of utilization of FWG as lightweight fill materials a) Reduction of settlement and preventation of slope failure of the embankment, b) Reduction of weight and soil pressure and the fill mountainous area, c) Reduction of differential settlement at the structure connection, d) Reduction of vertical soil pressure on the structure, e) Reduction of horizontal pressure on the two sides, f) Reduction of settlement and preventation of slope failure on soft ground

CHAPTER 3

MATERIALS AND EXPERIMENTAL ANALYSIS

3.1. Powders

The glass powder used in the expansion experiments and foam sample preparation for mechanical testing and thermal conductivity measurements was received from a glass polishing factory, Camex (Bursa, Turkey). The used powder was a residue of window glass polishing. The polishing was performed using SiC powder. In the grinding process, boron-based oil was applied as a coolant agent. A picture of as-received glass powder is shown in Figure 3.1(a). As-received glass foam powder is agglomerated as depicted Figure 3.1(a) as the powder was kept in an open area. The glass powder was pulverized using a Fritsch Disk Mill PULVERISETTE 13. The picture of the powder after pulverization is shown in Figure 3.1(b).

In the few foam expansion experiments, SiC particles (Aldrich-code 357391) with a particle size of <37 μm and an amount of 1 wt% was added to the powder as foaming agent. The SEM picture of the used SiC particles is shown in Figure 3.2. The foaming properties of a glass powder received from a local company and obtained by milling of the post-consumer and industrial glass waste was also investigated for comparison. The average powder size of this glass powder was 70 μm.

(a)

(b)

Figure 3.1. The picture of as-received glass powder, (a) before and (b) after pulverization.

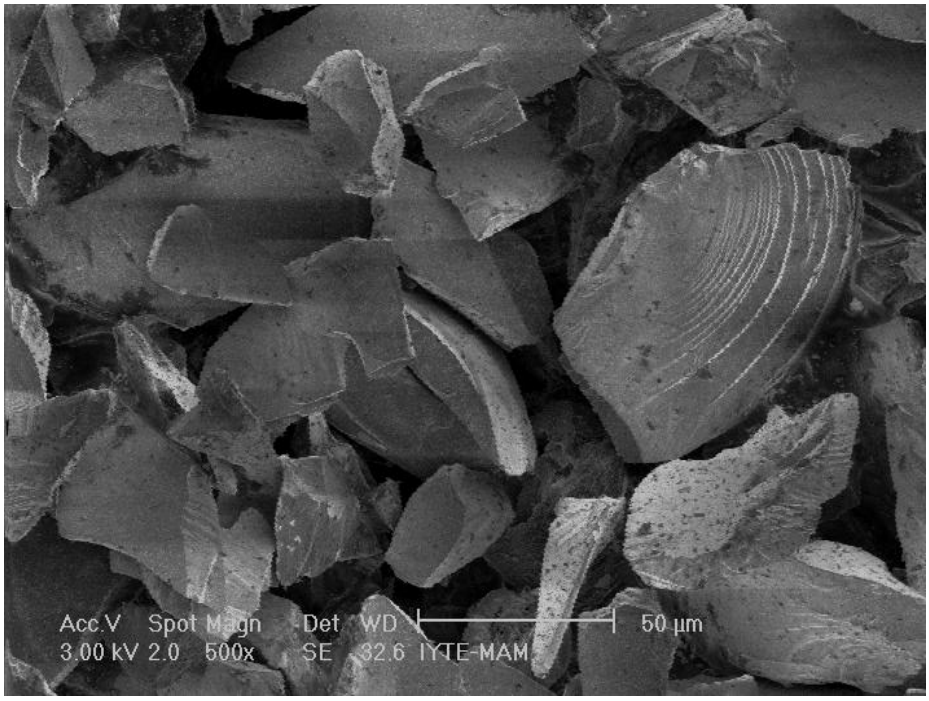

Figure 3.2. SEM picture of SiC particles.

3.2. Characterization

The particle size of the powder was measured by means of a Malvern Mastersizer 2000 particle size analyzer. The crystallographic structure of the powder and the foams was determined using a Philips X'Pert Pro X-Ray Diffraction (XRD) device (Cu-Kα radiation, λ=1.54 A° and 40 kV). The XRD analysis was conducted between 5 and 80^{o} in 2θ intervals. The FTIR analysis of the as-received powders and the

foam were performed using a using Shimadzu 8400S FTIR Spectrometer. The thermo-gravimetric analyses (TGA) of the powders were conducted using a Perkin Elmer Diamond TG/DTA device at 1200 °C maximum temperature. The elemental compositions were determined using a Spectro IQ II X-Ray Fluorescence (XRF) device. Scanning electron microscopy (SEM) was used to investigate the morphological properties of powders and foams. SEM images were taken in a FEI Quanta 205 FEG SEM in secondary electron mode (SE). The samples for microscopy were prepared by mounting the samples in Buehler epo-wick branded fast curing epoxy. Samples were grinded with Buehler Met-II SiC grinding papers through 800, 1000, 1200, 2000 and 2400 grids. Then, the samples were polished sequentially 9 μm, 6 μm, 3 μm and 1 μm diamond solution. The density of foams was determined by measuring the weight and dimensions of the test samples.

3.3. Foaming Set-Up and Foaming Experiments

The pulverized glass powder was mixed (in the case of SiC addition) in a Ball Mill for ½ h at 400 rpm using silica balls. The mixture was then compacted inside a cylindrical mold under a compaction pressure of 15 MPa. The compacts of 3 cm diameter and 7 mm thickness (Figure 3.3) were prepared for foam expansion experiments without using a binder.

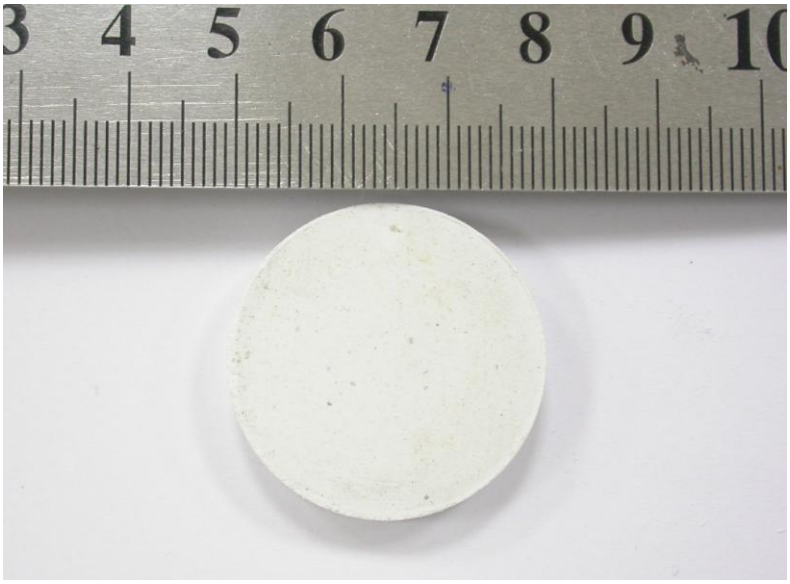

Figure 3.3. The picture of a glass powder compact for expansion experiments.

The schematic and picture of the front view of the foaming set-up are shown in Figures 3.4(a) and (b), respectively. The details of the experimental set-up used are given in [34]. Simply the set-up consisted of a vertical furnace, a linear expansion measurement system and a foaming mold. The bottom of the foaming mold (3 cm in diameter and 8 cm in height) was enclosed tightly and the compact was placed at the bottom of the mold. A linear variable displacement transducer (LVDT) was connected to the steel expansion rod through a wire and two pulleys. A thermocouple directly contacted to the bottom of the compact was used to measure the compact temperature during foaming. LVDT and thermocouple data were collected using a data logger (Data Taker DT 80).

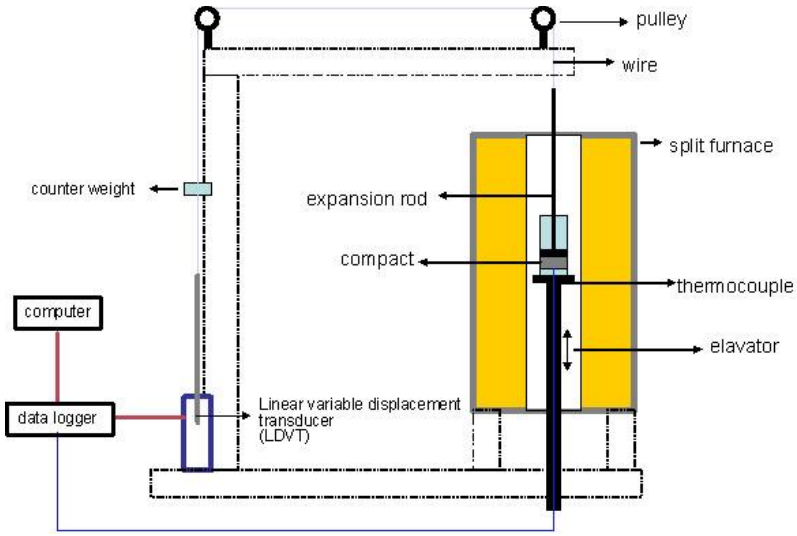

(a)

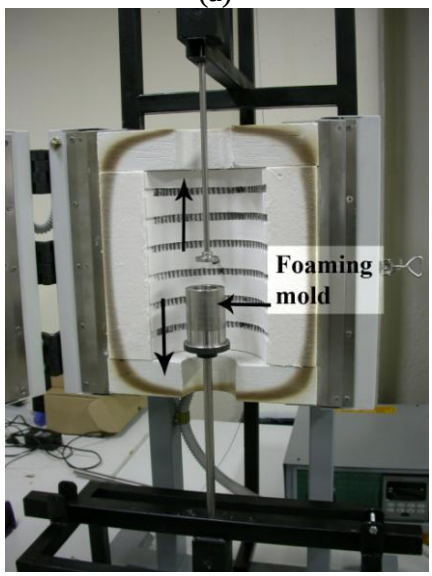

(b)

Figure 3.4. (a) Schematic of foam expansion measurement set-up and (b) foaming mold and sliding top and bottom rods.

In a typical experiment, the weight of the expansion rod is initially balanced using a counter weight for the expansion rod to apply minimum force possible on the foam during expansion (Figure 3.4(a)). Then, the furnace without foaming mold is heated to the prescribed temperature. Afterwards, the foaming mold accompanying the compact is inserted into the furnace by means of an elevator. After the compact insertion into the furnace, the top expansion rod connected to LVDT is lowered until the rod bottom head touches the compact surface.

A typical expansion-temperature-time and temperature-time graph is shown in Figure 3.5. As soon as the mold is inserted, the furnace temperature decreases to ~100 ^{o}C and then increases gradually in ~5 min as the mold is heated up. It is noted in Figure 3.5, the foaming starts at about 679 ^{o}C. As the compact expanded, the linear expansion measuring wire moves backward and the movement is measured with the help of a data logger which is connected to the LVDT. After foaming, the foaming mold is taken out of the furnace with the help of the elevator and cooled for the foam to solidify. The linear expansion data (mm) is converted to volume percent expansion (V_E %) using the following equation:

$$V_E(\%) = \frac{h_f - h_0}{h_0} x100 \qquad (3.1)$$

The foaming experiments continued until about the maximum expansion.

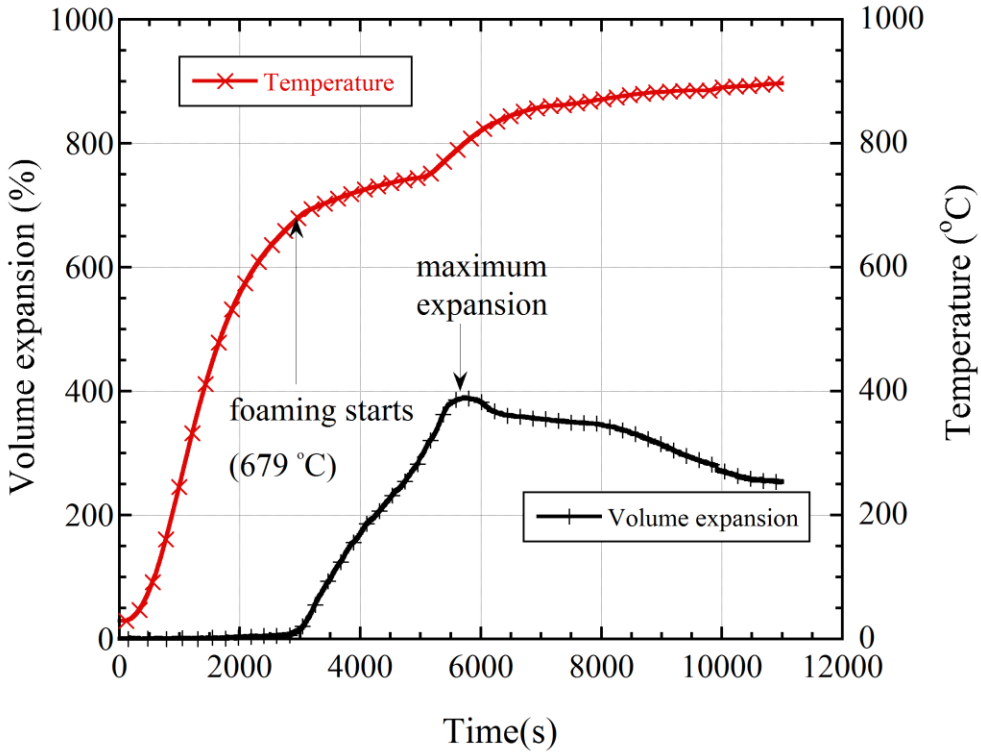

Figure 3.5. Typical glass powder expansion-temperature and time graph.

3.4. Foam Sample Preparation for Compression Testing and Thermal Conductivity Measurements

The foams for compression testing and thermal conductivity measurements were prepared by foaming 70x70x10 mm size compacts (Figure 3.6(a)). The compacts were prepared inside a steel die (Figure 3.6(b)) with a dimension of 70x70 mm under a pressure of 15 MPa. The powder compact was then placed inside a closed steel mold, which was coated with kaolin powder (Figure 3.7(a)). The kaolin prevented the reaction between the foamed glass and the mold. The expansion was limited to only the vertical direction. The foaming was performed using a Protherm Laboratory Furnace Model PLF 130/25 (Figure 3.7(b)). The foaming was performed at varying temperatures from 800°C to 925°C at 25°C intervals. The effect of heating rate was also investigated. Two heating rates were implemented; slow heating, 5°C/min and fast heating, 15°C/min. After foaming, the foam samples were cut into desired dimensions as depicted in Figures 3.8.

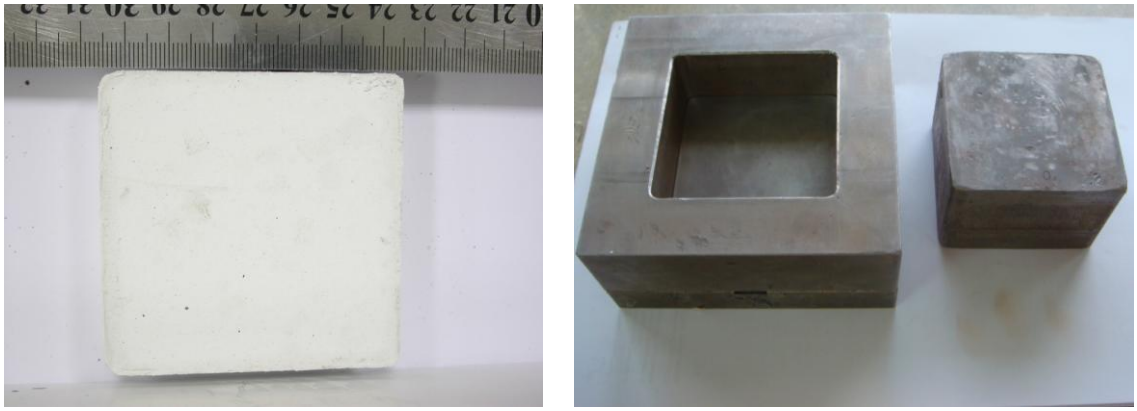

(a) (b)

Figure 3.6. (a) The glass powder compact for compression and thermal conductivity measurements and (b) steel die.

(a) (b)

Figure 3.7. (a) Koalin coated compact mold and (b) the furnace.

Figure 3.8. The foamed glass before (on the left) and after cutting (on the right).

3.5. Compression Testing and Thermal Conductivity Measurements

The compression test samples were prepared in accord with ASTM C240-97 standard and had the dimension of 50x50x50 mm (Figure 3.9(a)). Quasi-static compression tests were conducted using a displacement-controlled SHIMADZU AG-I universal tension-compression test machine with a cross-head speed of 2.5 mm/min, corresponding to a strain rate of $2x10^{-3}$ s^{-1}. The thermal conductivity tests were performed on the samples in 100x50x 10mm size (Figure 3.9(b)) using KEM QTM- 500 thermal conductivity detector.

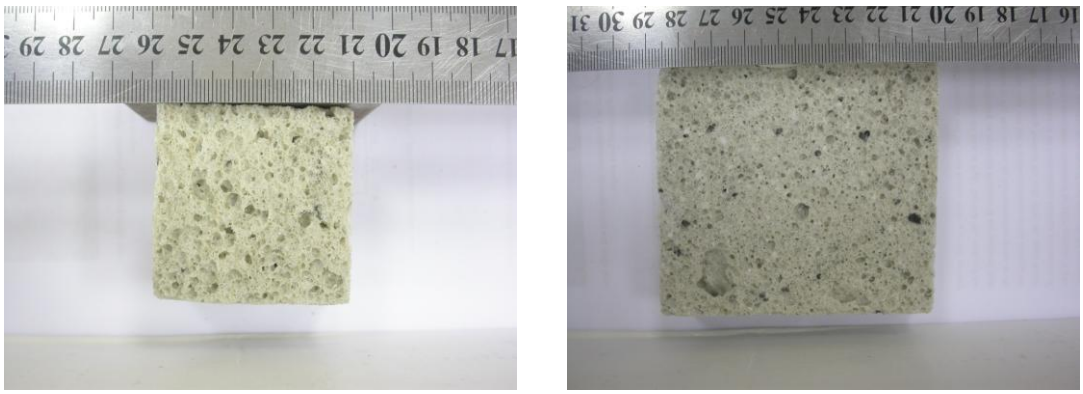

(a) (b)

Figure 3.9. (a) Compression foam test sample and (b) foam sample for conductivity measurements.

CHAPTER 4

RESULTS

4.1. Powder Characterization

The powder particle size analysis of as-received glass powder is shown in Figure 4.1. The particle size ranges between 5.695 μm (d_{10}) and 266.498 μm (d_{90}) with an average of 22.733 μm (d_{50}). The XRD results shown in Figure 4.2 confirm that the as-received powder is amorphous. The X-Ray Fluorescence analysis results of the glass powder are tabulated in Table 4.1 in oxide form assuming that all the elements are present as standard oxides. The results showed that the chemical compositions of the match with traditional window glass' chemical composition[35].

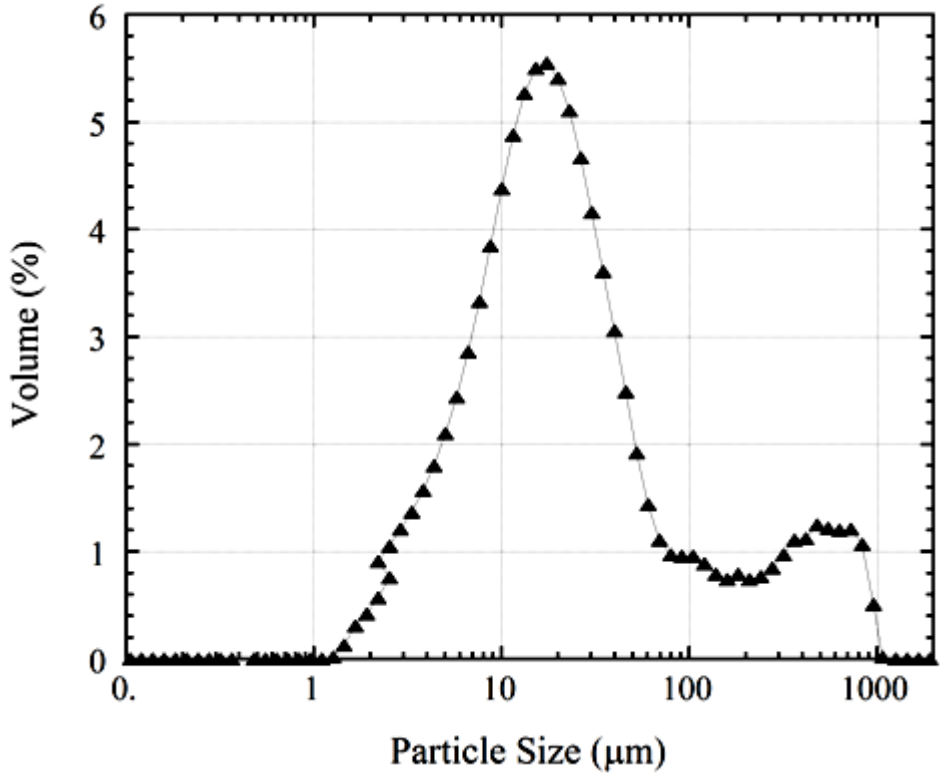

Figure 4.1. Particle size distribution of as-received glass powder.

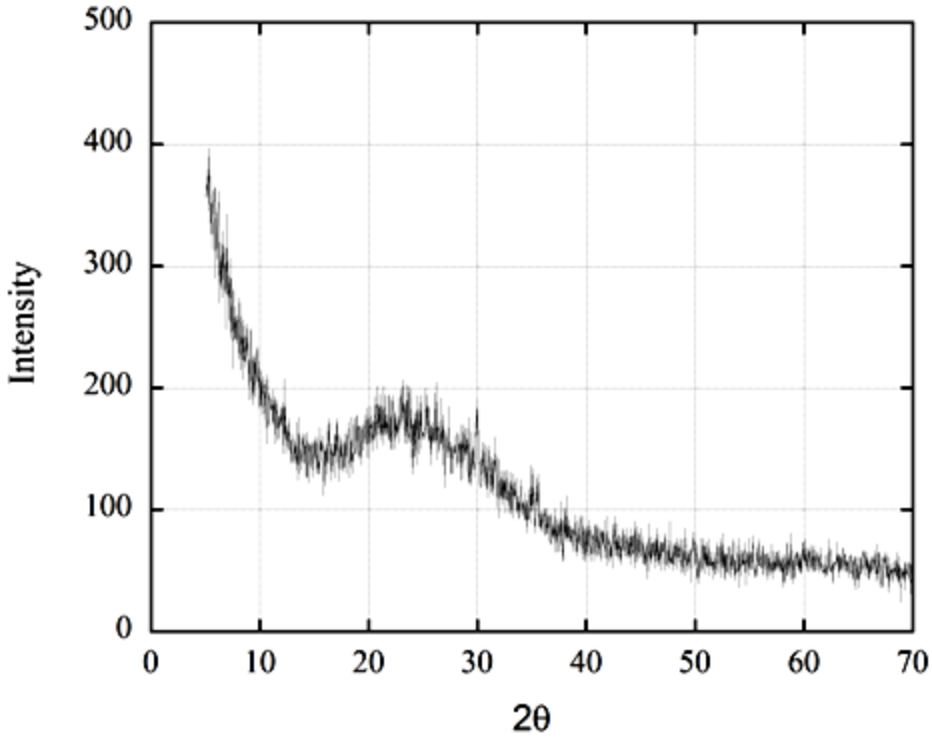

Figure 4.2. XRD spectra of as-received powder.

Table 4.1. Chemical composition of the glass powder determined by XRF.

Compound	SiO_2	Na_2O	CaO	MgO	Al_2O_3
Glass Oxide Concentration (As-received glass powder)	72.76%	11.18%	11.31%	1.74%	1.61%

Thermo-gravimetric analysis of glass foam powder and silicon carbide powder are shown in the Figures 4.3(a) and (b), respectively. The weight loss of glass powder is around 11wt % at 1200 °C. The weight loss continues until about 800 ^{o}C while the rate of weight loss decreases after melting of the powder, (~650°C). The decomposition of silicon carbide powder starts at 800 °C. The increased weight after 800 °C is due to the oxidation of SiC.

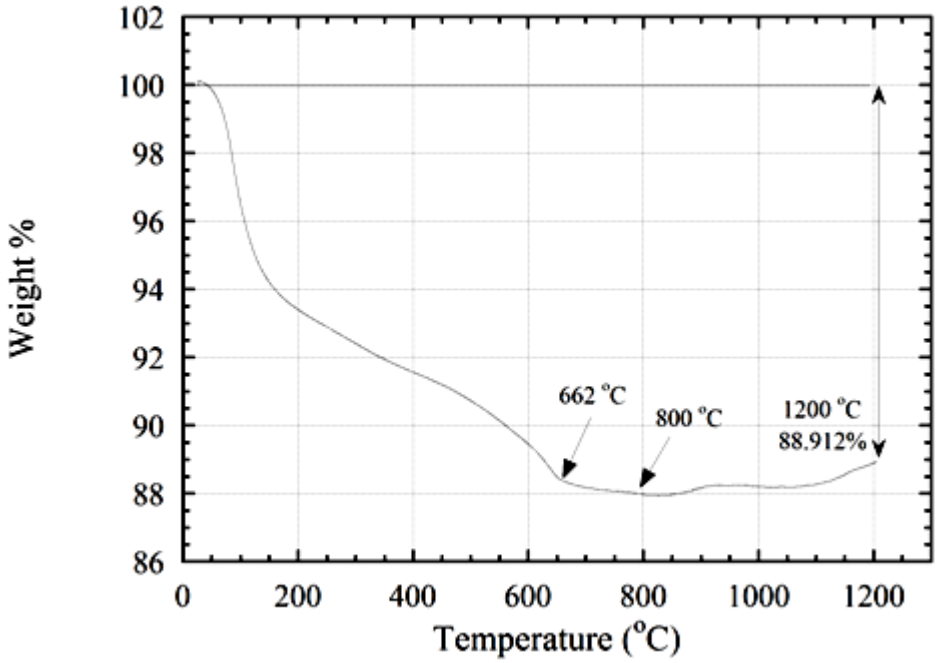

(a)

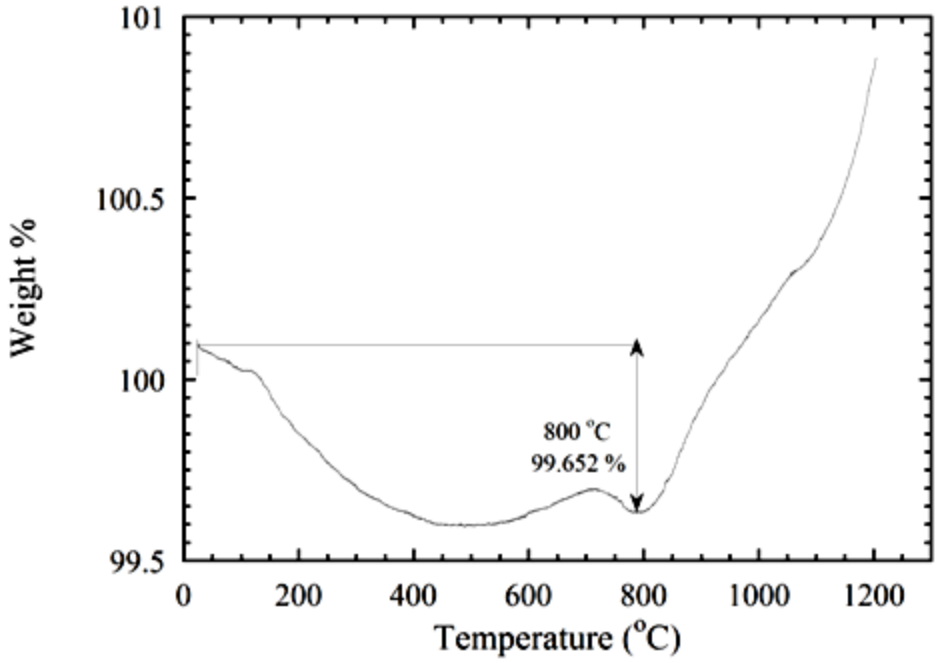

(b)

Figure 4.3. TGA curve of (a) glass and (b) SiC powder.

4.2. Characteristics of Glass Powder Compact Expansion

Figure 4.4 shows the volume expansion-temperature and time graphs of glass powder compacts at similar heating rates without blowing agent. The compact is quickly heated to 900 ^{o}C, thereafter the temperature became constant. In the same graphs the numbers correspond to the different stages of compact expansion. In region 1, the glass powder sinters as the temperature increases and then starts to expand, as a result of decomposition of a blowing agent presumably resulting in evolution of a gaseous product. The expansion of the glass powder sintered compact starts at about a characteristic temperature or at a temperature range between 695 and 705 ^{o}C. In region 2, a high expansion is seen and in this region the viscosity of the glass decreases to give gas expansion. The expansion reaches to a maximum at about 866-877 ^{o}C. The expansion in region 3 almost remains constant and thereafter it decreases gradually in region 4 and as the temperature of the foamed compact reaches the temperature of the furnace, the foam expansion tends to be constant at very long holding times. In these foaming experiments, the cooling rate is adjusted by closing the top hole of the tube furnace. In other foaming experiments the top of the furnace is kept open and the heating rate in these experiments is relatively lower. The maximum volume expansions vary between 700-772%. The maximum expansions are reached at about 2500 s after inserting the compact into the heated furnace. It is also noted that a small variation in the heating rate affect the expansion values of the compact as seen in Figure 4.4. Increasing heating rate increases the maximum expansion values. It is further noted that as-received powder expands itself without the addition of any blowing agent. This will be elaborated in discussion section of the thesis.

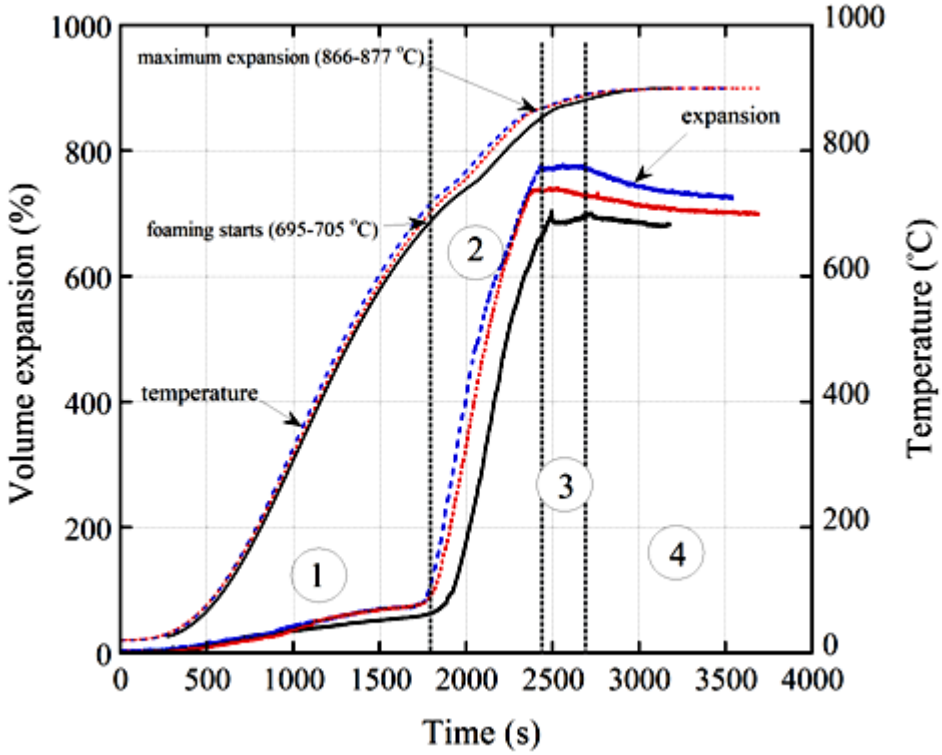

Figure 4.4. The volume expansion-temperature and time graphs of glass powder compacts at similar heating rates; the numbers corresponding to different stages of the compact expansion.

4.3. Effect of Holding Temperature on the Expansions of Powder Compacts

Figure 4.5(a) shows the expansion-temperature and time curves of glass powder compacts at different holding temperatures, from 700 to 925 ^{o}C. In these experiments, compacts are heated with same heating rate to the holding temperature. The heating rate in the experiments is relatively high as the top of the split furnace is closed. The results of this expansion studies is summarized as follows. As the holding temperature increases the expansion increases. It is noted that during heating to holding temperature the expansion is high and the expansion increases with time during holding until about 800 ^{o}C. At higher holding temperature the expansion almost remain to be constant. Therefore the optimum foaming temperature is between 800-825 ^{o}C for the studied glass powder. The expansions are around 600%: the compact thickness increases 6 times after foaming. Figure 4.5(b) show log expansion-temperature curves of the powder compacts. The compacts show very similar expansion-temperature curves. As

noted in the figure, the foaming starts at about 680 °C, when all expansion curves are considered.

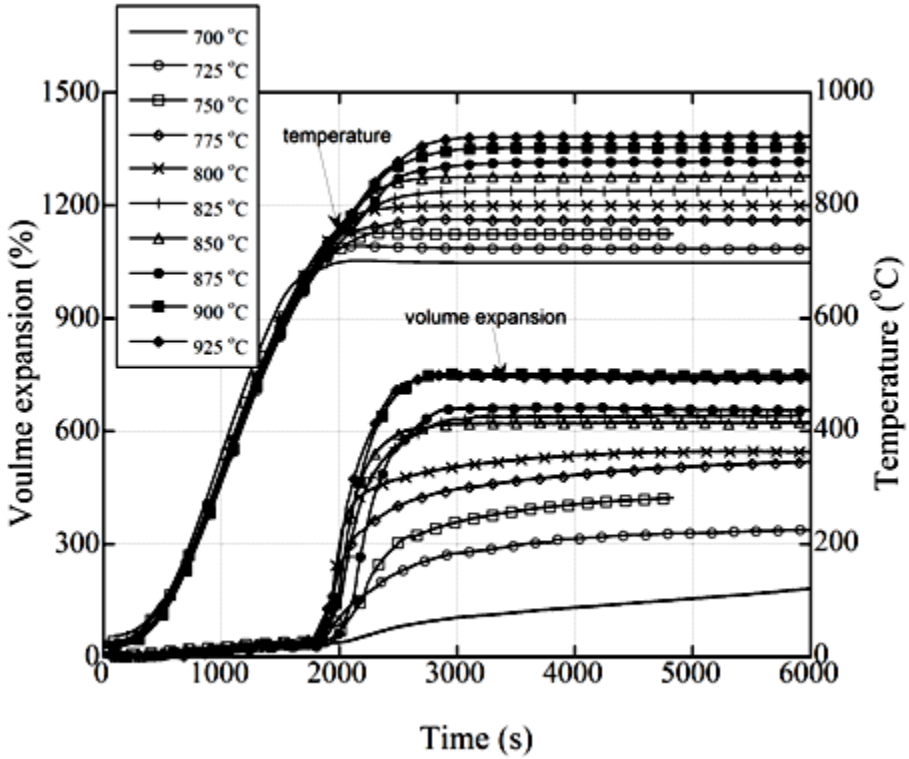

(a)

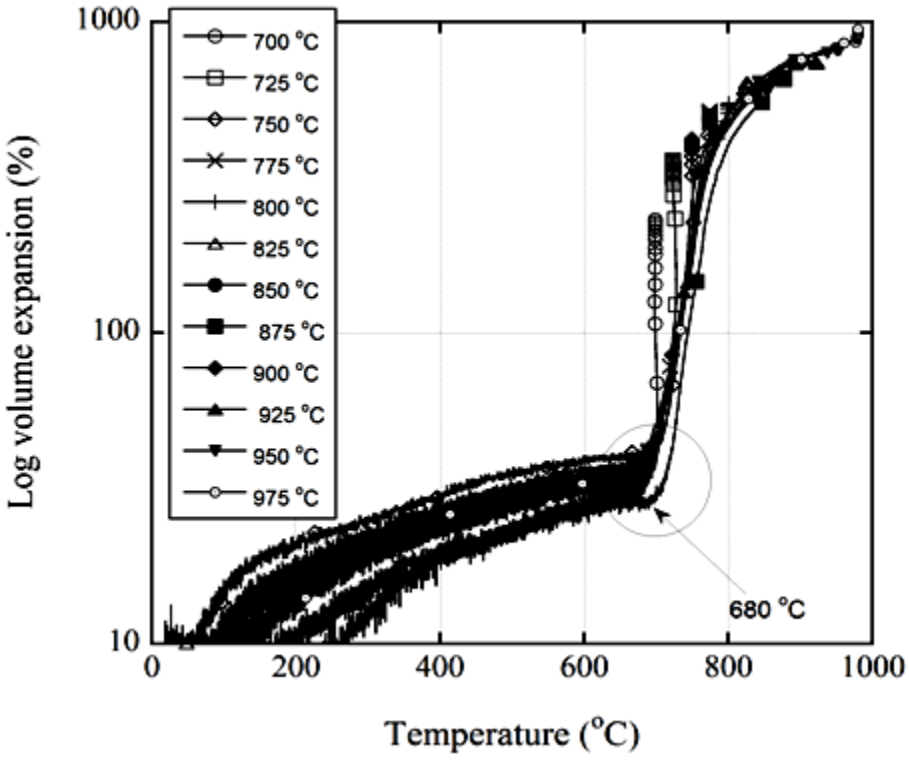

(b)

Figure 4.5. (a) Expansion vs. time and (b) temperature –expansion curves at different holding temperatures.

4.4. Effect of Heating Rate on the Expansions

Selected expansion-time and temperature-time graphs of the powder compacts foamed with different heating rates/schedules are shown in Figure 4.6. Increasing foaming temperature increases the expansions, while high heating rates results in higher expansions initially. It is also noted that slow heating rates results in lower expansions.

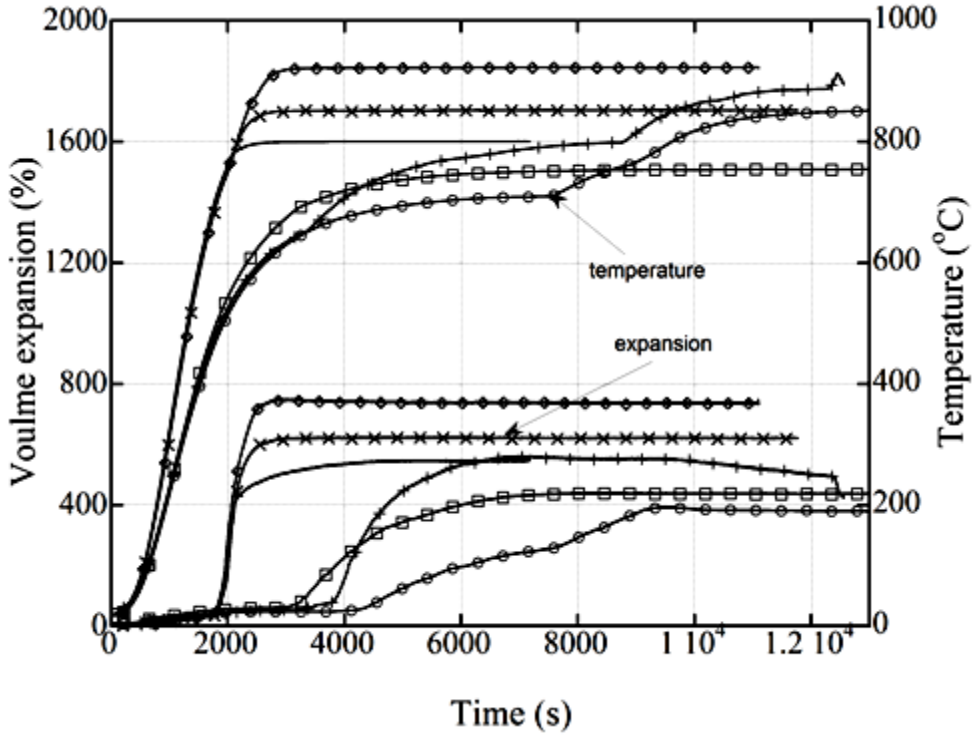

Figure 4.6. The expansion vs. time curves at different heating regimes

4.5. Effect of SiC Addition

The effect of SiC (1 wt%) on the expansion behavior of glass powder compacts is shown in Figure 4.7(a). The SiC addition at the similar heating schedules increases the expansion values as compared with powder compact without blowing agent addition. It is noted that in both compacts with and without SiC, the expansion starts at the same temperature, while initially the compact with SiC expands rapidly than those without SiC addition and reaches higher maximum expansion values. The effect of heating rate on the compacts with SiC addition is shown in Figure 4.7(b). Similar to compact without blowing agent, SiC added compacts show a heating rate dependent

expansion behavior. Higher heating rates end up with higher maximum expansion values.

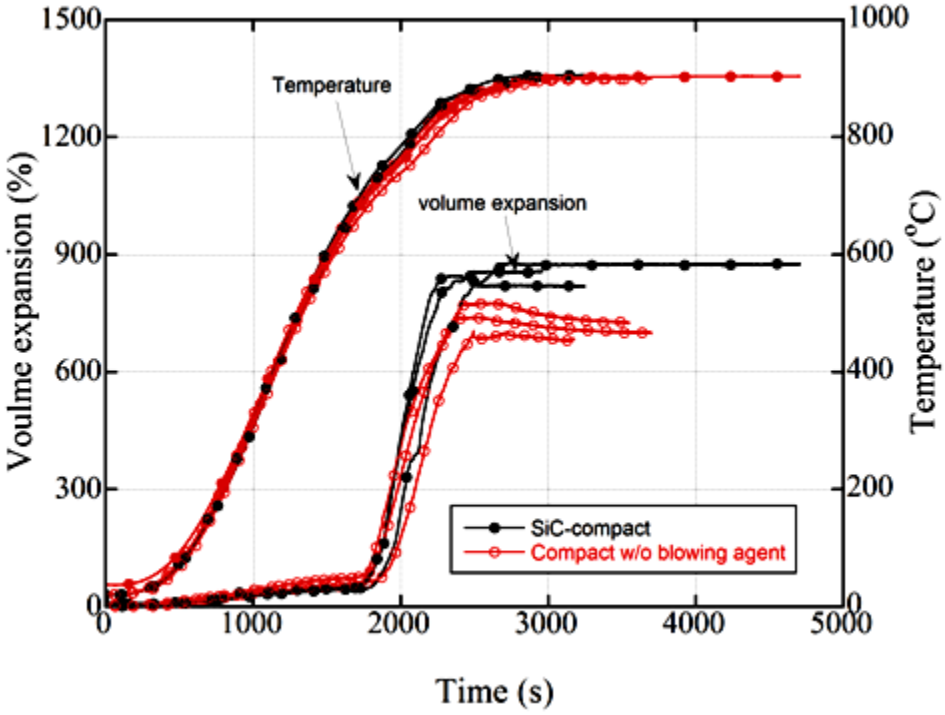

(a)

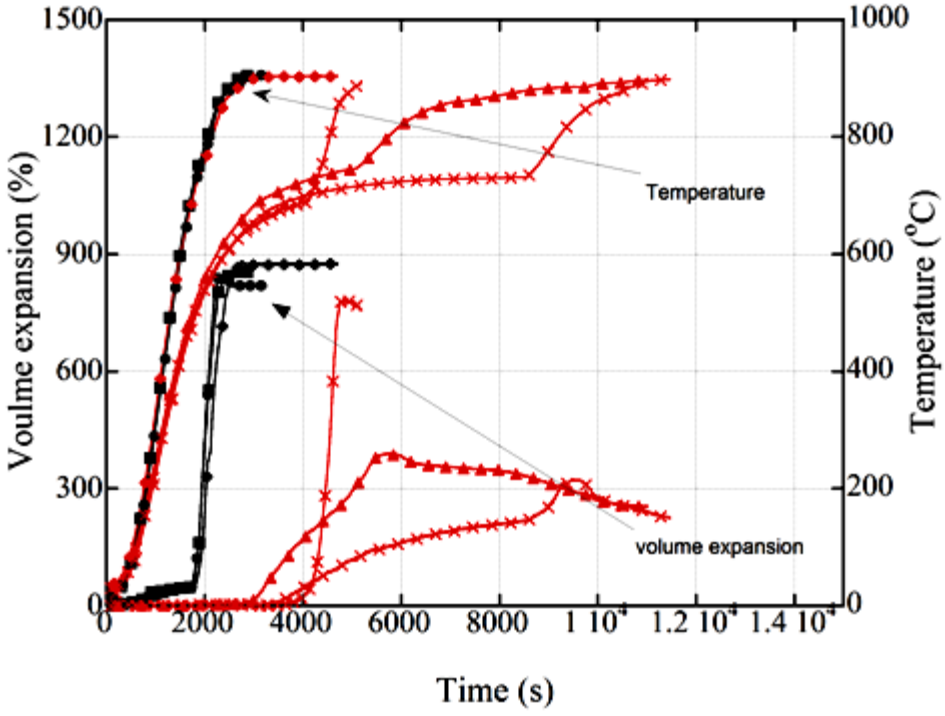

(b)

Figure 4.7. (a) The effect of SiC addition and (b) heating rate on the glass powder compacts.

4.6. Microstructure

The cell structure of powder compacts foamed at 750, 800 and 850 ^{o}C are shown sequentially in Figures 4.8(a-c). The foams were prepared by inserting the foaming mold into a preheated furnace with holding the mold for ½ h in the furnace. At 750 ^{o}C the size of the pores are relatively small and small pores and distributions of the pores are inhomogeneous. At 800 °C, the pores start to become coarser with sphere-like shapes. With increasing temperature to 850 ^{o}C, the sizes of the cells increase further. It is also noted that the cells are open, the cell walls accommodates inner connections with neighboring cells. The cell structure of powder compacts foamed at 900, 925 and 950 ^{o}C are shown sequentially in Figures 4.9(a-c). At increasing foaming temperature, the cells become elliptical and the cells start to coalesce due to thinning of pore walls. The elliptical shape of the cells causes lowering the volume of the sample, which means the density of the foam glass increases.

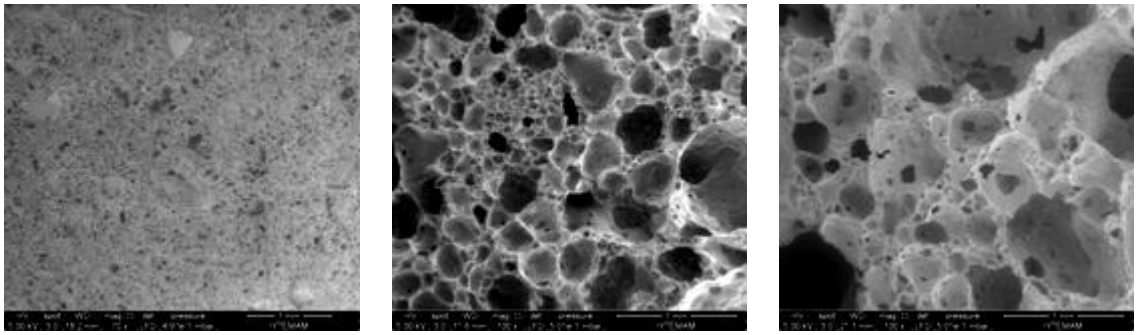

(a) (b) (c)

Figure 4.8. SEM image of the foamed glass sample at (a)750, (b) 800 and (c) 850 °C.

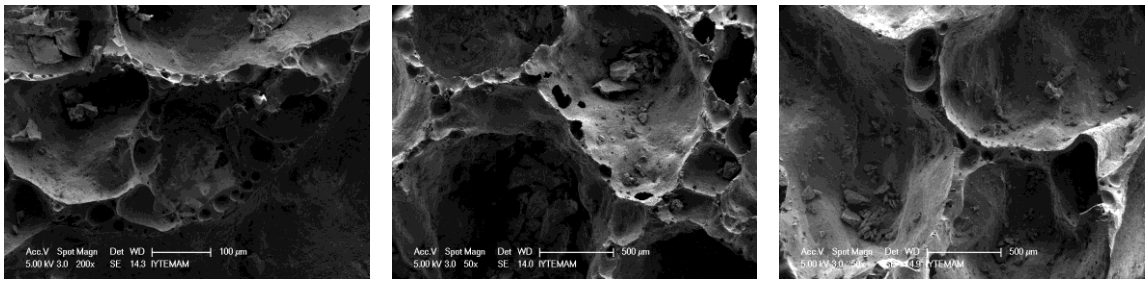

(a) (b) (c)

Figure 4.9. SEM image of the foamed glass sample at (a) 900, (b) 925 and (c) 950 °C.

The bottom and cross-section pictures of the foam processed using container glass waste powder and boron oil as blowing agent are shown in Figures 4.10(a) and (b). Similar to foam processed using polishing waste, these foams have dense skin layer on the surface. The cells are thicker at the bottom due to the drainage as depicted in Figure 4.10(b).

(a)

Figure 4.10. (a) The bottom and (b) cross-section pictures of the foam processed using container glass waste powder and boron oil as blowing agent.

(cont. on next page)

(b)

Figure 4.10 (cont.)

4.7. XRD

The XRD spectra of the foams prepared at various foaming temperatures are shown in Figure 4.11 together with the XRD spectrum of as-received glass powder. The intensity values are given as arbitrary units for comparison. In the XRD pattern of the foam prepared at 750, 800, 850 and 900 °C, the crystalline quartz peaks are seen at 21.41° and 35.45 ° (PCPDFWIN card 76-0931). Above 800 °C, two additional peaks of crystalline phases; wollastonite ($CaSiO_3$, PCPDFWIN card 02-0689) and diopsite ($MgCaSi_2O_6$, PCPDFWIN card 11-0605) are seen.

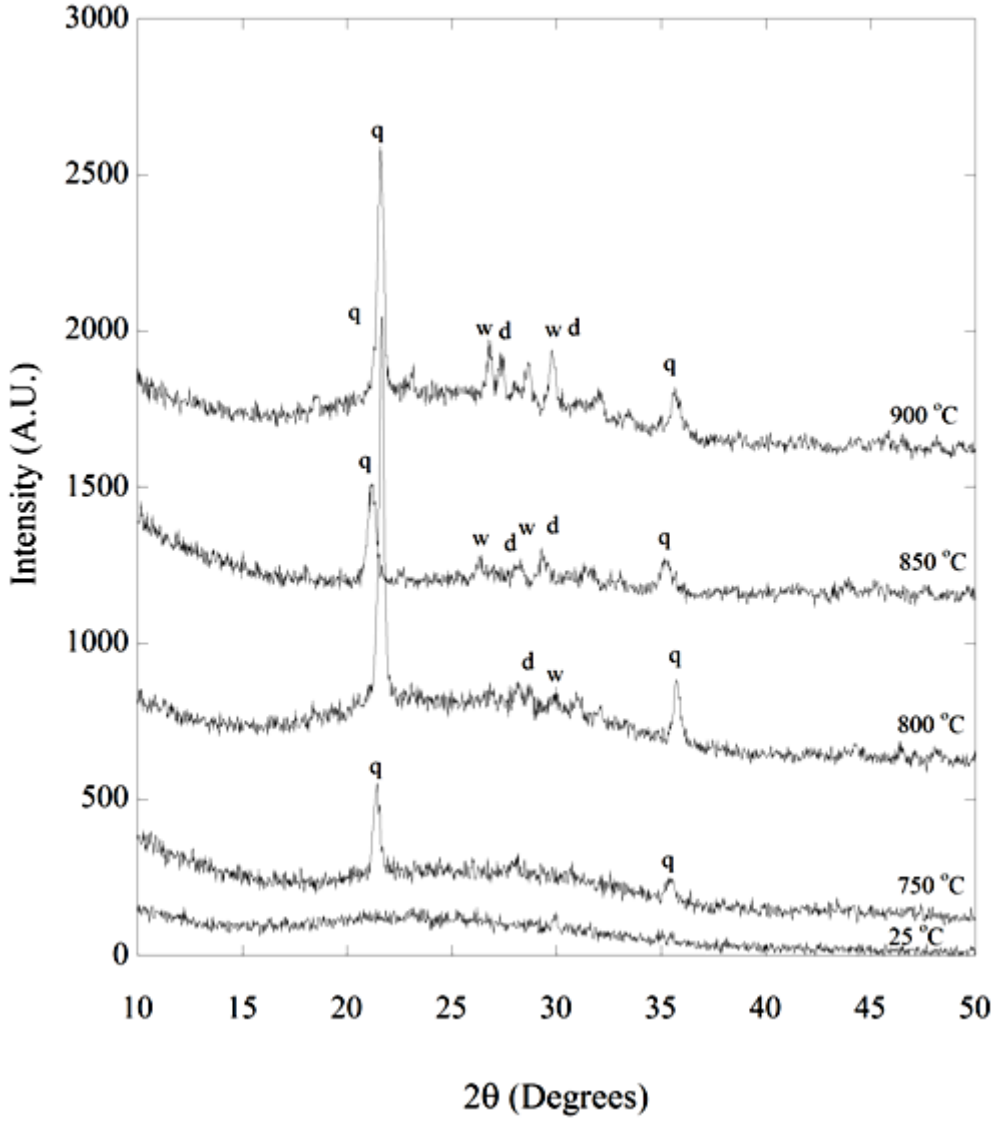

Figure 4.11. XRD patterns of glass foam powder at various temperatures

4.8. Compression Properties

The compressive stress-strain curves of the foam prepared with slow (5°C/min), and fast heating (15°C/min) rates are shown in Figures 4.12(a) and (b), respectively. All foam samples showed brittle characteristics, following the collapse stress (maximum stress) the sample fractured catastrophically. The corresponding density, collapse stress and plateau stresses of the foam prepared with slow and fast heating are tabulated in Table 4.2 and Table 4.3, respectively. As the foaming temperature increases, the final density of the foam decreases for both heating rates. Accordingly, the collapse and plateau stresses decrease as the foam density decreases.

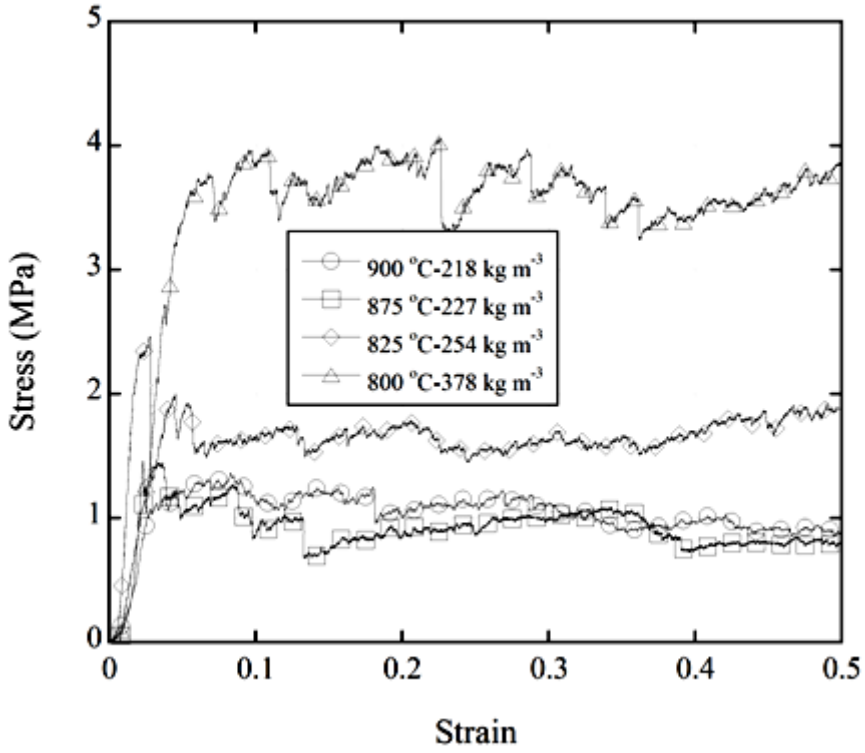

(a)

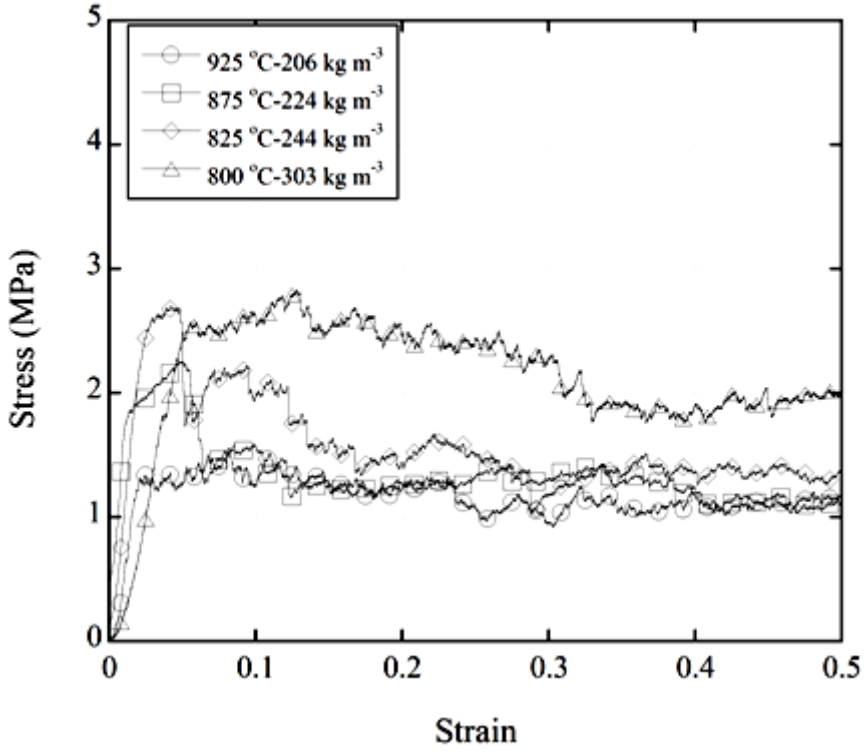

(b)

Figure 4.12. Compressive stress-strain curves of the foam prepared by (a) slow and (b) fast heating.

Table 4.2. Compression test results for slow heating rate

Temperature (°C)	Density (kg/m^3)	σ_y (MPa)	σ_{pl} (MPa)
800	378	4	3.5
825	254	2.6	2
850	244	2.4	1.7
875	227	2.2	1.6
900	218	1.4	1.1
925	211	0.9	0.7

Table 4.3. Compression test results for fast heating rate

Temperature (°C)	Density (kg/m^3)	σ_y (MPa)	σ_{pl} (MPa)
800	303	2.7	2.2
825	244	2.5	1.7
850	237	1.9	1.3
875	224	1.5	1.1
900	210	1.3	1
925	206	0.7	0.5

4.9. Thermal Conductivity

The foam sample densities used in the thermal conductivity measurements are tabulated in Table 4.4. The thermal conductivity measurements results are further tabulated in Table 4.5. The thermal conductivities range between 0.05 and 0.079 W m^{-1} $K^{-1.}$ The highest thermal conductivity is measured for the dentist foam and the lowest for the lowest foam density. Similar to collapse stresses the thermal conductivity increases with increasing foam density.

Table 4.4. The densities of foamed glass with respect to temperature and heating rate.

Temperature (°C)	Density (kg/m^3) Slow Heating Rate	Density (kg/m^3) Fast Heating Rate
800	378	303
825	254	244
850	244	237
875	227	224
900	218	210
925	211	206
950	247	238

Table 4.5. The thermal conductivity values of foamed glass with respect to temperature and heating rate.

Temperature (°C)	Thermal Conductivity (W/m*K)	
	Slow Heating Rate	Fast Heating Rate
800	0.079	0.073
825	0.068	0.065
850	0.062	0.059
875	0.057	0.053
900	0.0515	0.05
925	0.05	0.048
950	0.063	0.058

4.10. FTIR Analysis

Figure 4.12 shows FTIR analysis results of boron oil added glass powder, glass powder and glass foam powder after reaction. In Figure 4.12, the broad strong band located between 3600-3200 cm^{-1} is attributed to O-H stretching. The bands located at 2960-2800 cm^{-1} are arising from C-H stretching vibrations of aldehyde group. The broad peak located at 1660 cm^{-1} is stretching vibration of C-C. The peak located at 1460 cm^{-1} belongs to asymmetrical stretching of CH group. Also, the peak located at 1500 cm^{-1} indicates the aromatic structure of C=C [36]. The main strong peak located at 1050 cm^{-1} and the shoulder peak at 1200 cm^{-1} are attributed to asymmetrical stretching of Si-O-Si bonds.[37] The low frequency band (400-500 cm^{-1}) is attributed to rocking motion of Si-O-Si bridges, whereas the corresponding bending mode is responsible for adsorption at 700-850 cm^{-1}.[38]

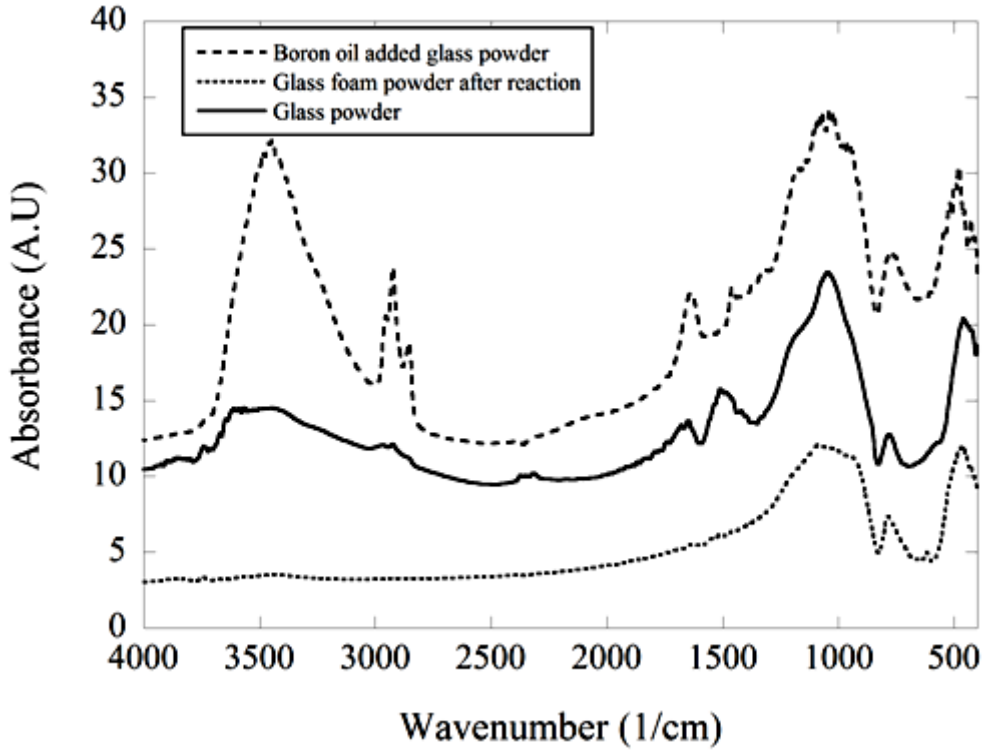

Figure 4.13. FTIR graph of glass foam powder, glass foam and boron oil added glass powder.

CHAPTER 5

DISCUSSIONS

5.1. Particle Size of Waste Glass Powder

The average particle size of the as-received waste glass powder was determined as 22.733 μm. The present thesis study did not aim to investigate the effect of particle size on the foaming and foamed glass microstructure; therefore, the as-received glass powder was directly used to make foamable powder compacts. However, it was previously shown that the glass powder size and the blowing agent powder size affected the cell size of foamed glass [39].

5.2. XRD and XRF Analyses

The XRD analysis of the as-received waste glass powder (Figure 4.2) exhibited an amorphous structure, which was typically found in the soda-lime window glass [35]. Furthermore, the XRF analyses results tabulated in Table 4.1 are well matched with the traditional window glass chemical composition tabulated in Table 5.1 [35].

Table 5.1. Chemical compositions of soda-lime glass for windows.

Oxide	**SiO_2**	**Na_2O**	**CaO**	**MgO**	**Al_2O_3**
Concentration %	71-73 %	12-14 %	10-12 %	1-4 %	0.5-1.5 %

5.3. TGA Curves, Weight Losses and Foaming

Figure 5.1 depicts the TGA curves of the as-received glass powder, conventional waste window glass powder and 10 wt% boron oil mixed with conventional waste window glass powder, together for comparison. As stated before, the as-received glass powder losses physical water (4 wt%) at about 100 °C. When the temperature increases to 600 °C the weight loss increases to 10 wt%. As the temperature increases up to

1200 °C, the weight loss increases to 11 wt%. It is noted that the weight of the glass powder melt does not change after 800 °C, while a small weight gain is seen after 850 °C. The weight loss between 100 °C and 800 °C occurs because of the burning of organic compounds of boron oil as will be elaborated later in this chapter (evolution of H_2O and CO_2). This is also reflected in the TGA curve of typical waste glass powder mixed with 10 wt% boron oil. The weight loss of boron oil continues until about 800 °C. The total weight loss is about 9 wt% at 800 °C. The increased weight of the as-received powder after 1000 °C is due to the oxidation of the molten glass. The same increase is also seen in the TGA curve of typical waste glass powder.

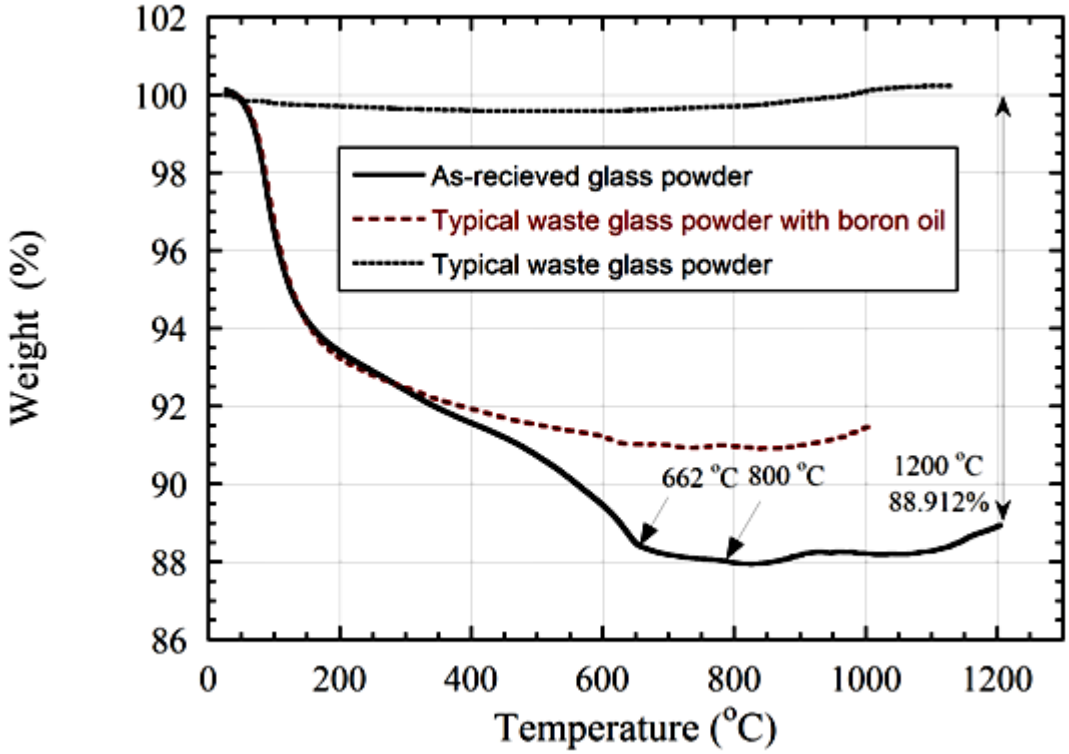

Figure 5.1. TGA curves of as-received powder, typical waste window glass powder and 10 wt% boron oil mixed typical waste window glass powder.

The weight losses of the compacts after foaming were also found to be very similar to those of TGA curves. The weight losses of the compacts before and after foaming at the prescribed foaming temperatures are tabulated in Table 5.1. The weight loss between 750 and 950 °C is about 11 wt% on the average and found to be not significantly affected by the foaming temperature as tabulated in Table 5.2.

Table 5.2. The weight losses of the compacts with foaming temperatures.

Sample	Heating Temperature (°C)	Initial Weight (g)	Final Weight (g)	Weight Loss (%)
1	750	100	88.9	11.1
2	800	100	89	11
3	850	100	89.1	10.9
4	900	100	89.1	10.9
5	950	100	89.1	10.9

Silicon carbide (SiC) is the most widely used foaming agent for foamed glass production [40]. The initial oxidation of SiC was presumed to start at about 800 °C as depicted in Figure 4.3(b). The weight gain of SiC powders in the TGA curve of Figure 4.3(b) is noted to be parabolic over 1100 ^{o}C. The weight gain is due to the reaction:

$$SiC+2O_2 \rightarrow SiO_2+CO_2 \quad (5.1)$$

as shown in a previous study [41]. Therefore it is expected that the extensive foaming of the glass compacts with SiC blowing agent should start after about 800 ^{o}C.

5.4. Expansion Behavior of the Compacts

Typical volume expansion-time and temperature-time graphs of the foamed glass powder compact consist of 4 different regions as marked in Figure 4.4. These are 1) Region 1: the sintering region, 2) Region 2: the expansion region, 3) Region 3: the maximum expansion and 4) Region 4: the final region in which expansion vanishes. Initially a slight increase in the volume of the compact occurs until about 700 °C in Region 1. The expansion is due to the thermal expansion of the pellet. The transition from Region 1 to Region 2 occurs at 695 °C (marked with arrow in Figure 4.5). The transition point indicates the temperature at which the foaming starts. This temperature also corresponds to the principle of foam glass process that is between 700 and 900 °C. The glass powder forms into a viscous liquid and then the foaming agent decomposes to

form a gas, in turn forms bubbles. As the temperature increases, the volume expansion also increases. The expansion reaches a maximum value (maximum volume expansion) at about 866 ^{o}C in Region 2. The volume expansion does not change significantly in Region 3. In Region 4 the expansion vanishes.

The compacts expansion reached to a maximum in Region 2 in a short time, for the temperatures above 800 ^{o}C (see Figure 4.5(a)). The compact expansion continued in Region 2 until about very long furnace holding times when the temperature was 800 ^{o}C or lower. This result agrees well with the weight loss of the as-received powder after 800 ^{o}C. The volume expansion, pore growth and the viscosity of the glass foam powder compact strongly depend on temperature. On the other side, the foaming process started at 680°C independent of the furnace holding temperature (Figure 4.5(b)). The maximum volume expansion conducted at 800 °C was about 530 % while it was 810% at 925 °C. As depicted in Figure 4.5(b).

The volume expansion behavior was also observed visually. The foaming just starts at about 700 °C, and when the temperature increases to 750 °C, the compact starts to expand further (Figure 5.2(a) and (b)). As the temperature increases to 900 and 950 ^{o}C, the compact expands rapidly (Figure 5.2(c) and (d)). If the temperature is too high the bubbles will rise and the body will collapse and not form a foam body [42].

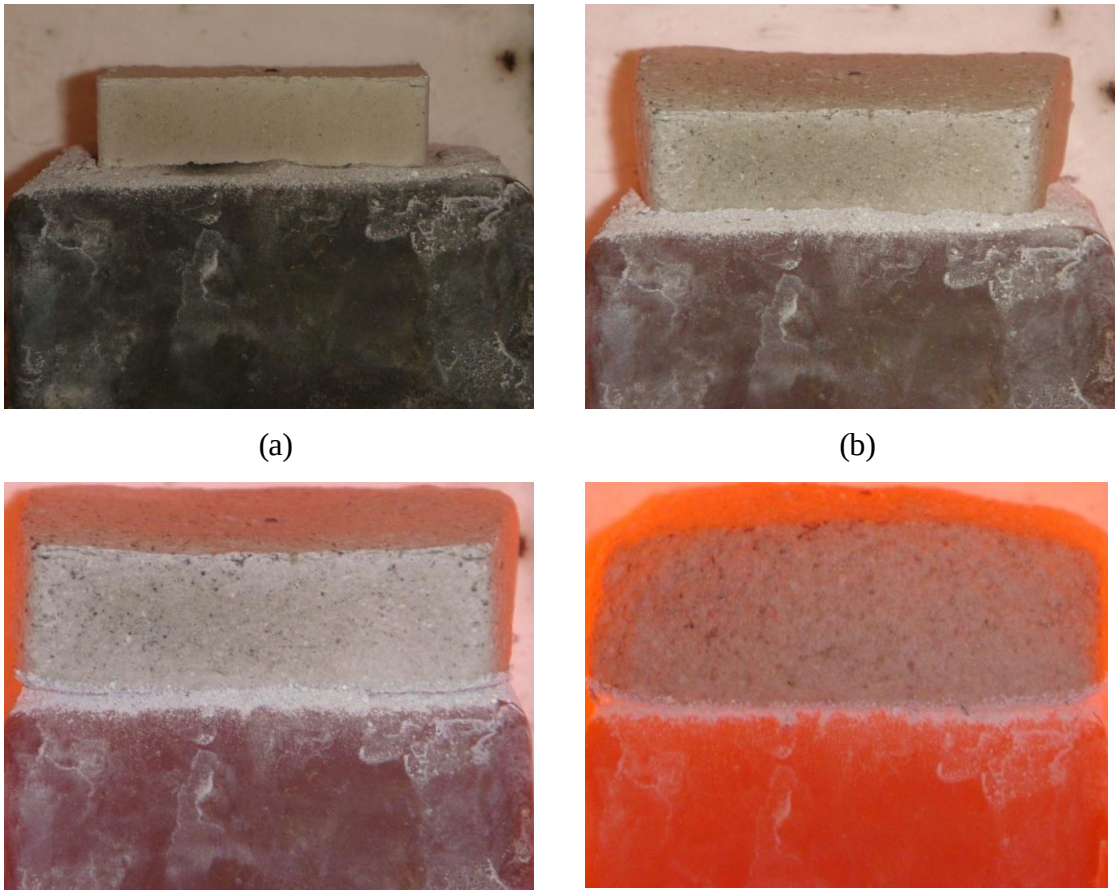

(a) (b)

(c) (d)

Figure 5.2. Glass foam powder compact (a) at 700 °C, (b) foamed glass at 750 °C, (c) at 900 °C and (d) at 950 °C.

The heating rate affected the foaming expansion (Figure 4.6). When the foaming temperature was below 800 ^{o}C, the expansion continued, while increasing temperature after a certain holding time reduced the expansion values as compared with the compact heated quickly above 800 ^{o}C. During quick heating, although the volume expansion at 900 °C (Figure 4.5) was 750 %, the volume expansion at slow heating rate was around 500 %. The same effect was also observed in SiC contained compacts (Figure 4.7(b)). The reduced expansion of powder compacts with slow heating rate was also shown in a previous study [10]. It was concluded that slow heating lead to early release of the gas from the foaming agent before the viscosity of the glass was low enough to allow the glass to expand rapidly and more gas escaped from within the body [11].

The effect of foaming temperature on the final relative density of the foamed glass is shown in Figure 5.3. The final relative densities are slightly lower when the heating rate is fast. The heating rate significantly affects the relative density at the

foaming temperature below 850 ^{o}C. Since the foaming agent, presumably boron oil, decomposes completely at about 800 °C, above that temperature the heating rate is expected not significantly affect the foam expansion. However, at the temperatures around 800 °C, the slow heating rate will allow a higher rate of gas escape from the compact. To reach higher expansions and lower relative densities, the compact should be heated quickly until about 800 °C.

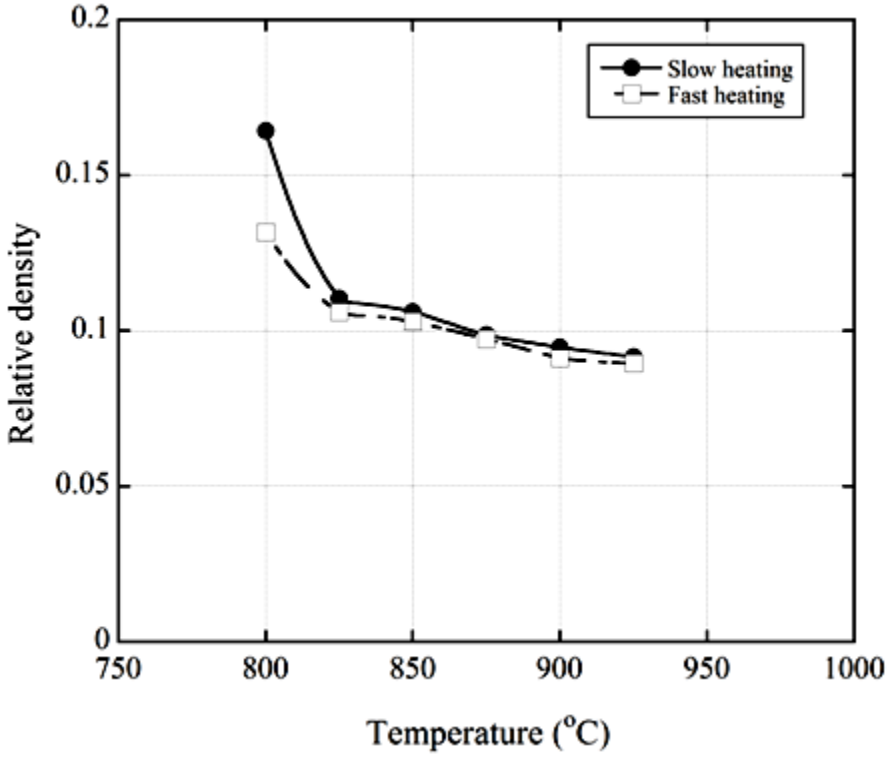

Figure 5.3. The relative density of foam as function of foaming temperature.

It was further shown that the addition of SiC did not affect the foaming starting temperature (Figure 4.7(a)). While the volume expansion of SiC-compacts, slightly higher than that of glass powder compacts.

The glass powder compacts were prepared under 15 MPa pressure. This value was selected since increasing the compaction pressure caused cracks on the surface and in the corners of the compact. The use of kaolin coated foaming mold powder prevented the reaction between the compact and the mold [43]. Furthermore, the thermal stability of kaolin was advantageous.

The foam evolution in the foaming powder compact process may be considered composing of several stages. The foam formation starts in the solid state just before the

melting of the compact. As the foam expands, the decaying processes become active with cell wall rupture, coarsening and drainage. The cell wall rupture results from the thinning of the cell walls: the liquid flows from the film surface (cell wall) to the plateau borders (cell edges) under the action of gravity and the pressure difference between film and plateau border. The drainage reduces the cell wall thickness and forms a dense layer at the bottom and the cell rupture induces larger cells at the top sections of the foam cylinder. The cell rupture time (T) was further approximated using the following relation;

$$T = \frac{b}{2}\sqrt{\frac{c\rho}{\sigma}} \tag{5.2}$$

where, b, c, ρ and σ are the cell wall length, thickness, liquid density and surface tension, respectively. Haibel et. al. [44] analyzed the possible stabilization mechanisms operative in the foaming powder compact process. In the case of no particles on plateau borders and cell walls, the liquid metal on a cell wall, under the effect of the pressure difference,

$$\Delta P = 2\sigma\left(\frac{1}{R_{PB}} - \frac{1}{R_F}\right) \tag{5.3}$$

flows from the cell walls to the plateau borders (R_{PB} and R_F are the radius of curvature of plateau border and cell face, respectively). The partially wetted particles on the cell wall form menisci of radius of $R_F \cong R_{PB}$, which reduces the pressure difference and capillary suction. The increased viscosity of the melt by the presence of small particles in the film may immobilize the liquid metal flow.

As the foaming time increases the cell walls become thinner, while cell edges become thicker due to the drainage. Figure 5.4(a) shows the compact microstructure at the very initial stage of foaming process. The cells are relatively small and the smaller cells are spherical in shape. As the foaming proceeds, the cells not only form but also change the shape from sphere to polyhedra (Figure 5.4(b)). This also causes to the thicker cell edges and thinner cell walls. The foam glass microstructure observations also revealed the presence of smaller pores on the cell edeges and cell walls as previously observed [27]. Figure 5.5(a) shows an SEM micrograph of fomed glass cell edge and cell walls. Small size pores on the cell edges and cell walls are clearly seen.

The boron oil is a neutralizer blowing agent, dissociating to give a gaseous product similar to dolomite ($CaMg(CO_3)_2$) and $CaCO_3$. The gas evolution burst the cell walls, forming interconnections between the cells. This effect is also seen in Figure 5.5(b), in which few torn cell walls are clearly seen. This will certainly increases the water absorption of the foamed glass as stated earlier.

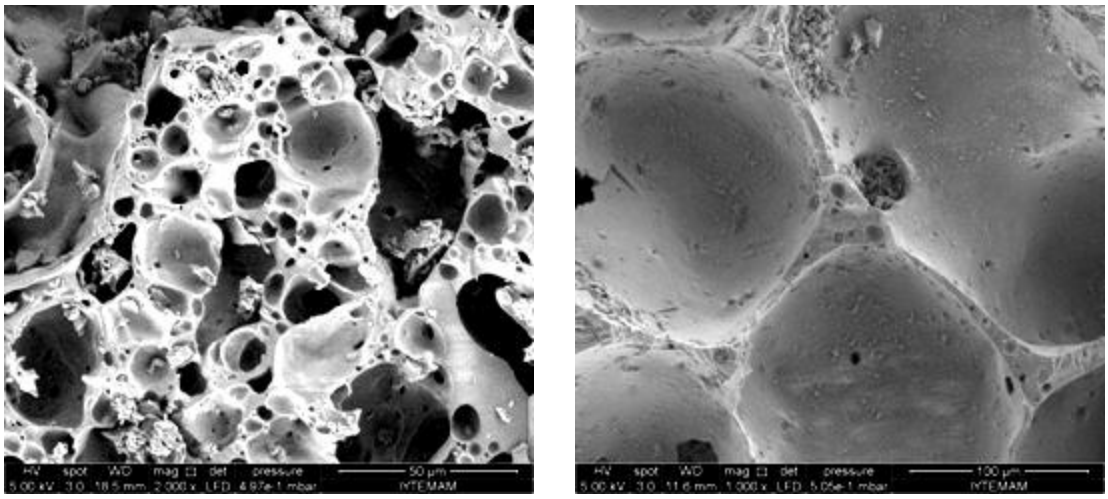

(a) (b)

Figure 5.4. SEM micrograph showing cells in a compact foamed at (a) initial foaming stage and (b) at maximum expansion.

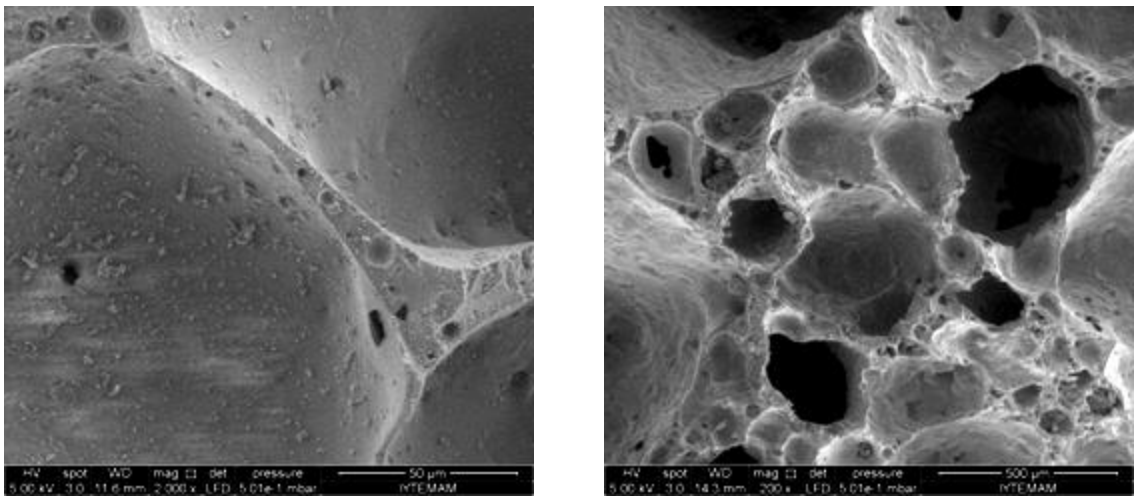

(a) (b)

Figure 5.5. SEM micrographs showing (a) small pores on the cell edges and cell walls and (b) interconnections on the cells walls.

The final macrostructure of the foamed glass is depicted in Figure 5.6. The macrostructure is very heterogeneous in cell size: small spherical pores are distributed around the large elliptical cells.

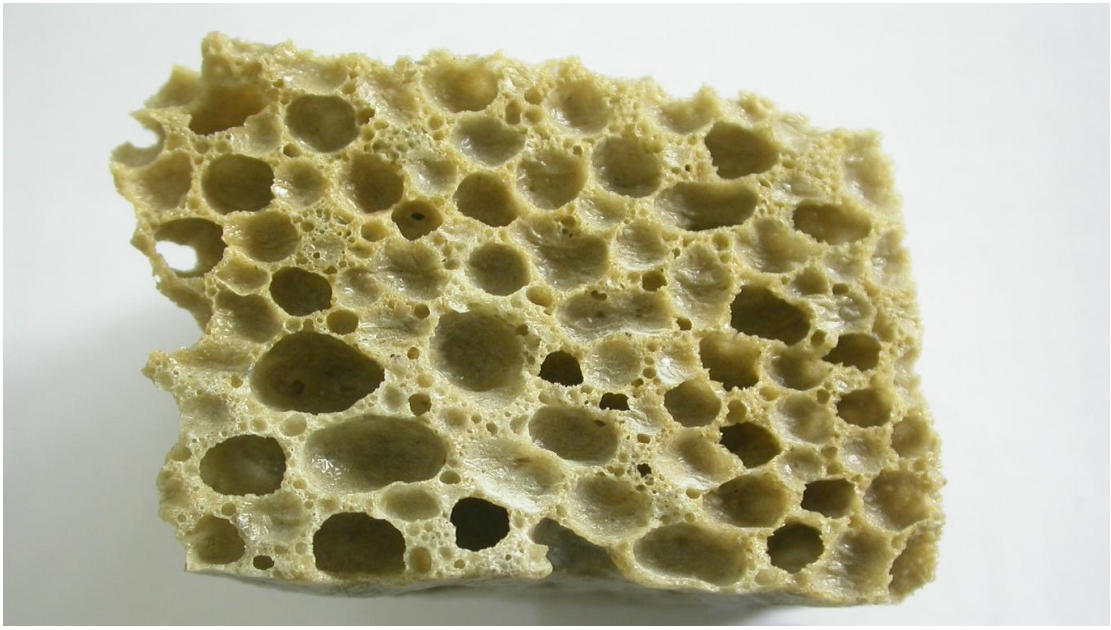

Figure 5.6. The foamed glass produced at 950 °C.

5.5. Crystallization

The foaming of the compact at 750 °C yielded the only crystalline phase of quartz (see Figure 4.11). As the foaming temperature increased, wollastonite and diopsite phases appeared. Increasing the temperature caused an increase of the intensity of the peaks. Wollastonite formation was due to the high content of CaO in the composition of glass, and it could be favored by the sintering temperature, close to the temperature of maximum crystallisation rate for the same phase [15]. Furthermore increasing the foaming temperature caused the crystallization of diopside between 800 and 900 °C. The XRD analysis result is also in a good agreement with the study of Tulyaganov et al [45]. Figures 5.7 (a) and (b) show the SEM cell pictures of the foamed compacts at 750 and 800 C, respectively. The needle-like features seen on the cell walls in Figure 5.7(b) are the wollastonite and diopsite crystals. The formation of these crystal phases were proven microscopically also.

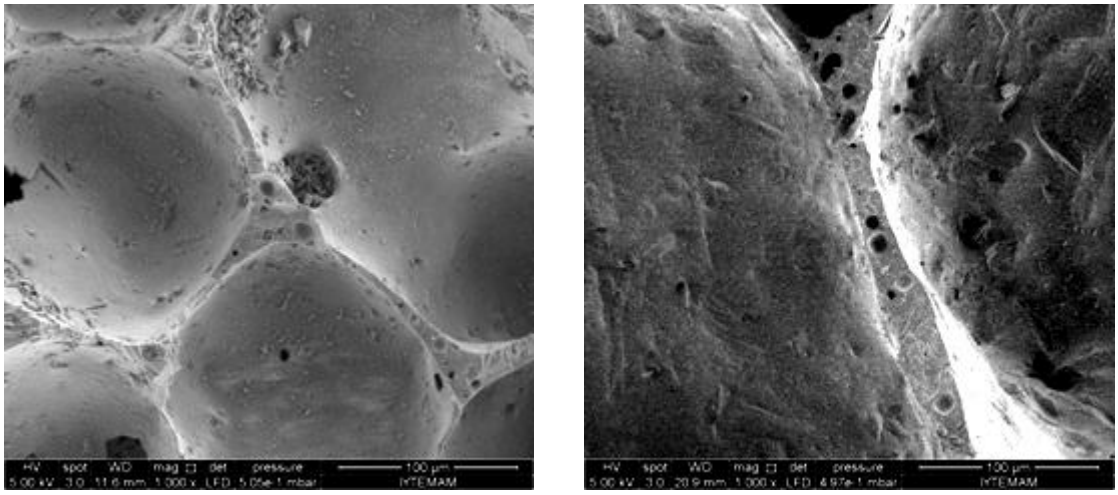

(a) (b)

Figure 5.7. Foamed glass cell SEM pictures after foaming at (a) 750 and (b) 800 °C.

5.6. Compressive Strength Results

Generally the higher the density of the foamed glass, the higher is the strength. This is due to the load is being distributed among a larger amount of glass. Both thin and closely spaced walls and sparse walls of greater thickness yielded higher strength [13]. For the studies on glass powder, no effect of heating rate was detected on the collapse and plateaus tresses. Figures 5.8(a) and (b) show the variations of collapse and plateau stresses with the relative density of the foamed glass, respectively. As the relative density increases both collapse and plateau stresses increase, while no significant effect of heating rate of foamed glass collapse and plateau stresses are seen in Figures 5.8(a) and (b). In the following analysis therefore the effect of heating rate is excluded and the foamed glass samples strength is analyzed only a function of relative density.

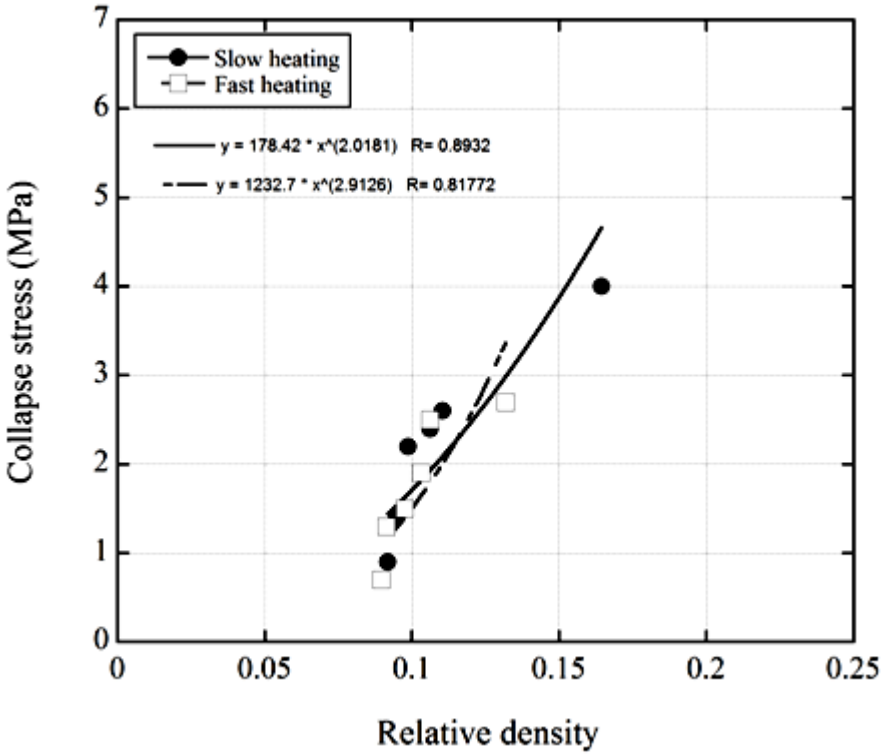

(a)

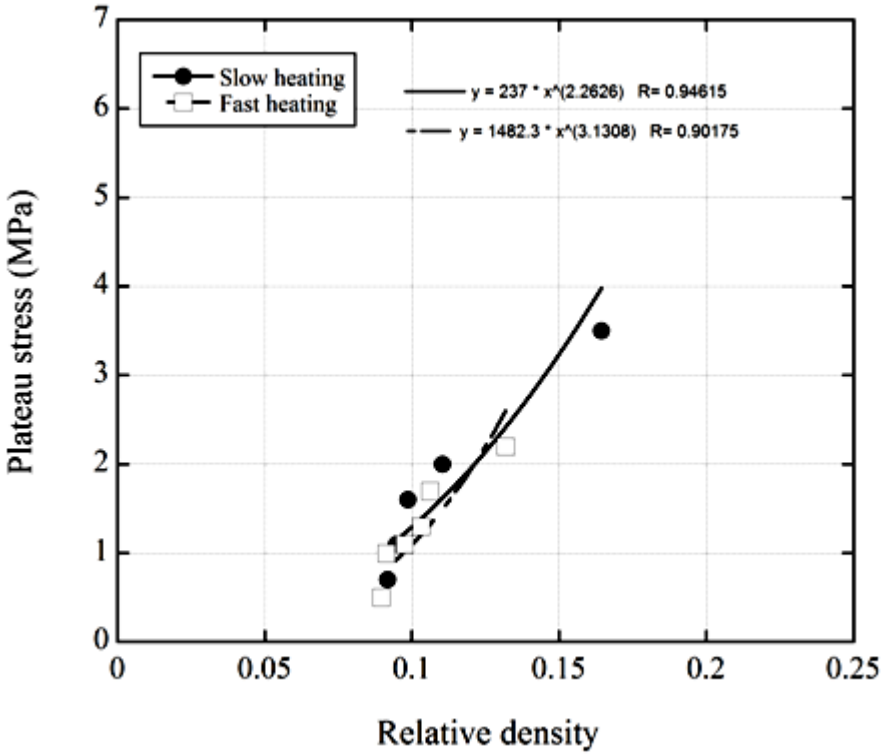

Figure 5.8. Variation of (a) collapse stress and (b) plateau stress with relative density for fast and slow heating rate.

The collapse and plateau stresses of the tested foamed glass foam is fitted with the equation given in previous chapter,

$$\sigma_f = \sigma_{bend}[C\sigma\phi\rho_{rel}^{3/2} + (1-\phi)\rho_{rel}] \quad (5.4)$$

In order to compare the strength of the foamed glass samples with the previously tested similar foams, the strength values taken from the literature are also fitted with Equation 5.4. The results of fitting are shown in Figures 5.9(a) and (b) for collapse and plateau stresses respectively. The fitting is performed for the ϕ values of 1, 0.9, 0.8, 0.7 and 1. For ϕ value of 1 and 0 refers to open and closed cell foams, respectively. It is noted in Figure 5.9(a), the collapse stress values of foamed glass fall between the ϕ values of 0.9 and 0.7. That means the foamed glass samples show a mechanical behavior near to open cell foams. This is also microscopically proven with the relatively thick cell edges. At low densities the foamed glass shows nearly open cell behavior as seen in Figure 5.9(a). This mainly because of majority of glass phase is collected at the cell edges. While at increasing densities the foam mechanical behavior switches from open cell to close cell behavior with increasing ϕ value. The same trends are also seen in the Plateau stress values in Figure 5.9(b).

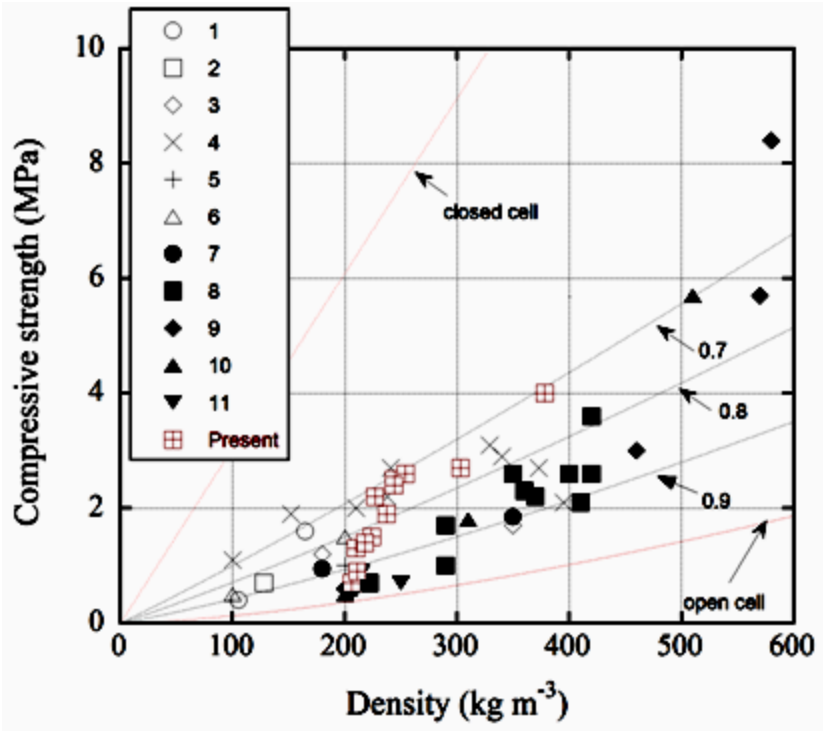

(a)

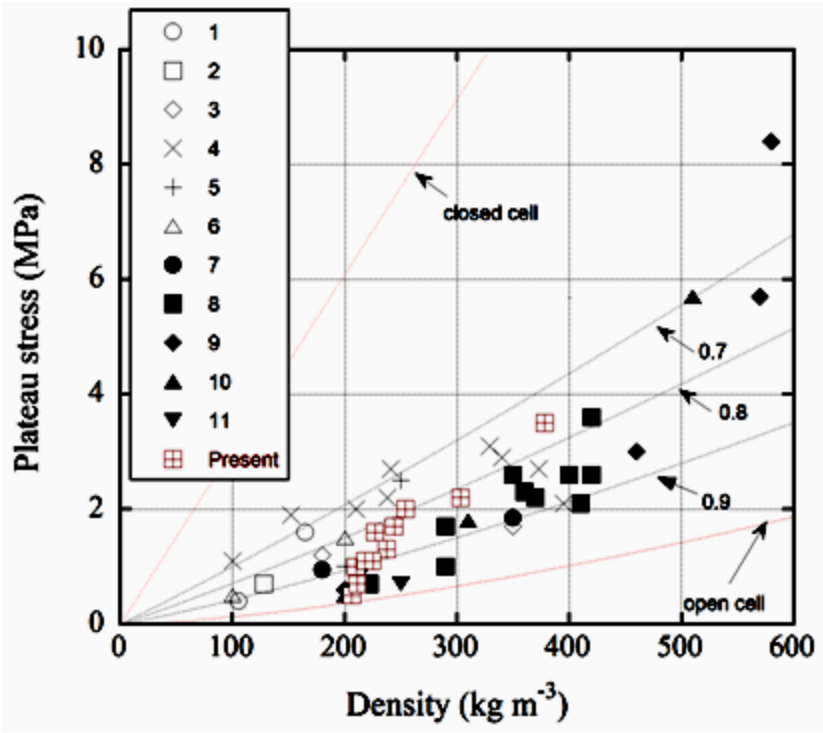

(b)

Figure 5.9. Fitting the (a) collapse stress and (b) plateau stress with Equation 5.4 with the present study and literature results.

5.7. Thermal Conductivity

Thermal conductivity of foamed glass also depends on the type of the porosity. Foamed glass with prevailing sealed pores is regarded as heat-insulating. The thermal conductivity also depends on the ratio between the solid and the pores [13]. The lower the density, the lower thermal conductivity is obtained. The variations in the thermal conductivity of the foamed glass samples with relative density for fast and slow heating show almost no effect of heating rate on the thermal conductivities as shown in Figure 5.10(a). The thermal conductivity is further noted to increase with increasing relative density. The present foam samples are also found to show similar thermal conductivities with the similar glass foams found in the literature (Figure 5.10(b)).

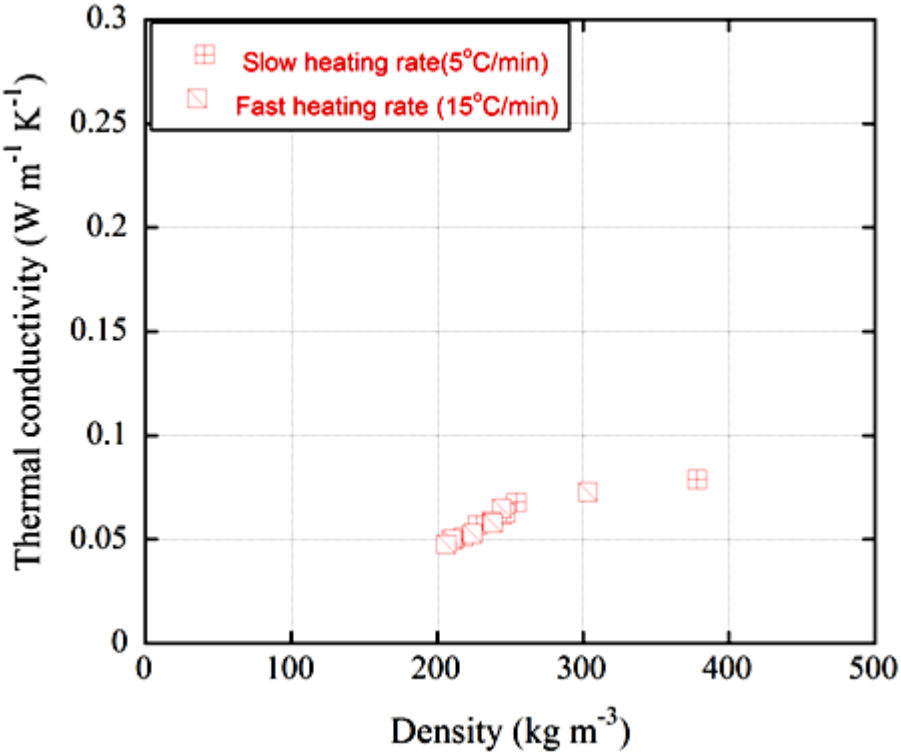

(a)

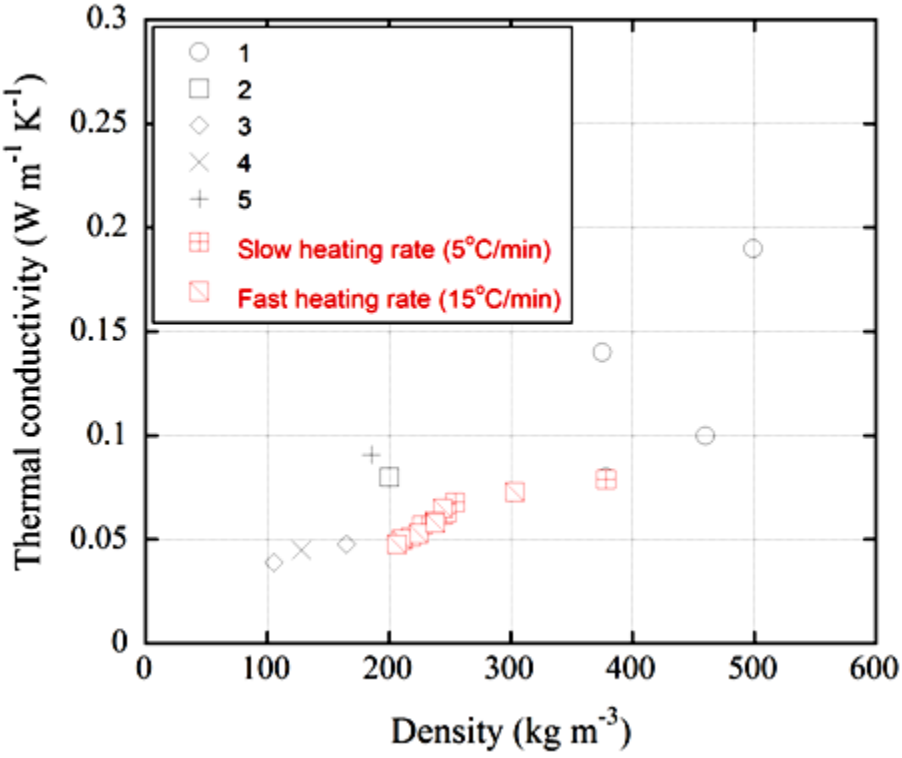

(b)

Figure 5.10. The variation thermal conductivity with density of (a) present foamed glass and (b) comparison with literature.

5.8. FTIR Analysis

The FTIR analysis of glass foam powder, waste glass powder with and without boron oil was shown in Figure 4.13. The wavelengths of the bonds found in the analysis tabulated in Table 5.3. The FTIR analysis of these three powder showed that, both boron oil added glass powder and glass foam powder had the same organic compound peaks. The peaks between 3600 and 1500 cm^{-1} in the FTIR analysis for glass foam powder are due to glass powder mixing with the boron oil during polishing of window glass.

Table 5.3. The wavelengths and the chemical bonds obtained in FTIR analysis

Chemical Bond	Wavelength (cm^{-1})
O-H	3600-3200
C-H	2960-2800
C-C	1660
C=C	1500
CH Group	1460
Si-O-Si	1050-1200
Si-O-Si	850-750
Si-O-Si	500-400

The exact amount of organic compounds and their chemical formula of boron oil within the glass foam powder are unknown. Common of all hydrocarbons, heating results in formation water vapor and carbon dioxide as,

$$C_nH_m + (m/4 + n)O_2 \rightarrow (m/2)H_2O + nCO_2 \quad (5.5)$$

It is presumed that the burning of the organic compounds during heating caused the self-foaming behavior of the as-received glass foam powder.

CHAPTER 6

CONCLUSIONS

In this study, the foaming behavior of a glass powder which is a residue from a window glass polishing factory in Bursa, was investigated at the foaming temperature between 700-950°C. As-received glass powder contained 72.76% SiO_2, 11.18% Na_2O, 11.31% CaO, 1.74% MgO and 1.61% Al_2O_3. The powder compacts for foaming experiments were prepared using a steel mold at the compaction pressure of 15 MPa. The foaming of the glass powder compacts was conducted in a foaming set-up, comprising a vertical furnace and a linear variable transducer which measured the linear expansion of the compacts. The compression tests and thermal conductivity measurements were performed on the foam samples of varying relative densities. Followings are concluded,

1. The XRD analysis of the as-received glass powder showed an amorphous structure of the as-received glass powder, which was typically found in soda-lime window glass.
2. The XRF analyses of the as-received glass were well matched with the traditional window glass chemical composition
3. The TGA analysis of the as-received powder showed no weight loss after about 800 °C. TGA curve of typical waste glass powder mixed with 10 wt% boron oil showed a similar TGA curve with as-received glass powder. The weight losses of the compacts after foaming between 750 and 950 °C was about 11 wt% on the average and found to be not significantly affected by the foaming temperature.
4. Typical volume expansion-time and temperature-time graphs of the glass powder compact consisted of 4 different regions, Region 1: the sintering region, Region 2: the expansion region, Region 3: the maximum expansion and Region 4: expansion vanishes. The maximum volume expansions and foam density varied between 700-772% and 0.378-0.206 g/cm^3, respectively.

5. The expansion of the glass powder compacts started at a characteristic temperature of 690-700 °C and reached a maximum volumetric expansion values at about 866-877 °C.
6. When the foaming temperature was below 800 ^{o}C, the compaction expansion continued in Region 2, while above that temperature the compact reached the maximum expansion in a relatively shorter time. The slow heating lead to early release of the gas from the foaming agent before the viscosity of the glass was low enough to allow the glass to expand rapidly and more gas escaped from within the body.
7. The heating rate affected the relative density at the foaming temperature below 850 ^{o}C. Above that temperature the heating rate did not affect the foam density.
8. The addition of SiC did not affect the foaming starting temperature (Figure 4.7(a)). While the volume expansion of SiC-compacts were found slightly higher than those of glass powder compacts without SiC addition.
9. XRD analysis after production the foamed glass showed that crystalline phases occurred as the foaming temperature increased. The foaming of the compact at 750 °C yielded the only crystalline phase of quartz. As the foaming temperature increased, wollastonite and diopsite crystals were formed.
10. The compressive strength of the prepared foams ranged between 1.9 and 3.9 MPa and the thermal conductivity between 0.048-0.079 W/K m.
11. Both collapse and plateau stresses increased with increasing relative density, while heating rate was not found to be affect the collapse and plateau stresses.
12. The foamed glass samples showed the mechanical behavior similar to open cell foams. This was attributed to the thicker cell edges and thinner cell walls leading to higher glass material accumulation on the cell edges.
13. The self-foaming behavior of the studied waste glass powder was attributed to the organic compounds within the boron oil which was used as a coolant in the polishing operations.

REFERENCES

[1] J. Lu and K. Onitsuka, "Construction utilization of foamed waste glass," *Journal of Environmental Sciences-China,* vol. 16, pp. 302-307, 2004.

[2] J. P. Wu, A. R. Boccaccini, P. D. Lee, M. J. Kershaw, and R. D. Rawlings, "Glass ceramic foams from coal ash and waste glass: production and characterisation," *Advances in Applied Ceramics,* vol. 105, pp. 32-39, Feb 2006.

[3] J. Hurley, "A Uk Market Survey For Foam Glass," The Waste and Resources Action Programme, The Old Academy, 21 Horsefair, Banbury, Oxon OX16 0AH2003.

[4] Wrap. (2011). www.wrap.org.uk.

[5] H. R. Fernandes, D. U. Tulyaganov, and J. M. F. Ferreira, "Production and characterisation of glass ceramic foams from recycled raw materials," *Advances in Applied Ceramics,* vol. 108, pp. 9-13, Jan 2009.

[6] K. K. Éidukyavichus, V. R. Matseikene, V. V. Balkyavichus, A. A. Shpokauskas, A. A. Laukaitis, and L. Y. Kunskaite, "Use of Cullet of Different Chemical Compositions in Foam Glass Production," *Glass and Ceramics,* vol. 61, pp. 77-80, 2004.

[7] V. A. Lotov and E. V. Krivenkova, "Kinetics of formation of the porous structure in foam glass," *Glass and Ceramics,* vol. 59, pp. 89-93, Mar-Apr 2002.

[8] N. M. Bobkova, S. E. Barantseva, and E. E. Trusova, "Production of foam glass with granite siftings from the Mikashevichi Deposit," *Glass and Ceramics,* vol. 64, pp. 47-50, Jan-Feb 2007.

[9] G. D. Jones, W. J. McMillan, and C. N. Williams, "Foamed Glass And Vitreous Silica Pellets," *Industrial & Engineering Chemistry Product Research and Development,* vol. 18, pp. 64-69, 1979.

[10] S. K. Goyal and I. B. Cutler, "Absorption of water in waste glass as a precursor for foam formation," *Journal of Non-Crystalline Solids,* vol. 19, pp. 311-320, 1975.

[11] V. E. Manevich and K. Y. Subbotin, "Mechanism Of Foam-Glass Formation," *Glass and Ceramics,* vol. 65, pp. 154-156, May 2008.

[12] B. Gerhard, "Foaming of borosilicate glasses by chemical reactions in the temperature range 950-1150°C," *Journal of Non-Crystalline Solids,* vol. 38-39, Part 2, pp. 855-860, 1980.

[13] Y. A. Spiridonov and L. A. Orlova, "Problems of foam glass production," *Glass and Ceramics,* vol. 60, pp. 313-314, Sep-Oct 2003.

[14] H. R. Fernandes, D. U. Tulyaganov, and J. M. F. Ferreira, "Preparation and characterization of foams from sheet glass and fly ash using carbonates as foaming agents," *Ceramics International,* vol. 35, pp. 229-235, 2009.

[15] E. Bernardo, R. Cedro, M. Florean, and S. Hreglich, "Reutilization and stabilization of wastes by the production of glass foams," *Ceramics International,* vol. 33, pp. 963-968, 2007.

[16] E. Bernardo, G. Scarinci, P. Bertuzzi, P. Ercole, and L. Ramon, "Recycling of waste glasses into partially crystallized glass foams," *Journal of Porous Materials,* vol. 17, pp. 359-365, Jun 2010.

[17] A. Pokorny, J. Vicenzi, and C. P. Bergmann, "Influence of heating rate on the microstructure of glass foams," *Waste Management & Research,* vol. 29, pp. 172-179, Feb 2011.

[18] F. Mear, P. Yot, M. Cambon, and A. M. Ribes, "Elaboration and characterisation of foam glass from cathode ray tubes," *Advances in Applied Ceramics,* vol. 104, pp. 123-130, Jun 2005.

[19] E. Bernardo, G. Scarinci, and S. Hreglich, "Foam glass as a way of recycling glasses from cathode ray tubes," *Glass Science and Technology,* vol. 78, pp. 7-11, Jan-Feb 2005.

[20] F. Mear, P. Yot, and M. Ribes, "Effects of temperature, reaction time and reducing agent content on the synthesis of macroporous foam glasses from waste funnel glasses," *Materials Letters,* vol. 60, pp. 929-934, Apr 2006.

[21] F. Mear, P. Yot, R. Viennois, and M. Ribes, "Mechanical behaviour and thermal and electrical properties of foam glass," *Ceramics International,* vol. 33, pp. 543-550, 2007.

[22] H. W. Guo, Y. X. Gong, and S. Y. Gao, "Preparation of high strength foam glass-ceramics from waste cathode ray tube," *Materials Letters,* vol. 64, pp. 997-999, Apr 2010.

[23] E. Bernardo and F. Albertini, "Glass foams from dismantled cathode ray tubes," *Ceramics International,* vol. 32, pp. 603-608, 2006.

[24] Z. Matamoros-Veloza, J. C. Rendon-Angeles, K. Yanagisawa, M. A. Cisneros-Guerrero, M. M. Cisneros-Guerrero, and L. Aguirre, "Preparation of foamed glasses from CRT TV glass by means of hydrothermal hot-pressing technique," *Journal of the European Ceramic Society,* vol. 28, pp. 739-745, 2008.

[25] M. J. Chen, F. S. Zhang, and J. X. Zhu, "Lead recovery and the feasibility of foam glass production from funnel glass of dismantled cathode ray tube through pyrovacuum process," *Journal of Hazardous Materials,* vol. 161, pp. 1109-1113, Jan 2009.

[26] A. S. Apkar'yan, V. G. Khristyukov, and G. V. Smirnov, "Granulated foam glass ceramic - A promising heat-insulating material," *Glass and Ceramics,* vol. 65, pp. 74-76, Mar 2008.

[27] D. U. Tulyaganov, H. R. Fernandes, S. Agathopoulos, and J. M. F. Ferreira, "Preparation and characterization of high compressive strength foams from sheet glass," *Journal of Porous Materials,* vol. 13, pp. 133-139, Apr 2006.

[28] A. I. Shutov, L. I. Yashurkaeva, S. V. Alekseev, and T. V. Yashurkaev, "Study of the structure of foam glass with different characteristics," *Glass and Ceramics,* vol. 64, pp. 297-299, Sep 2007.

[29] O. V. Kaz'mina, V. I. Vereshchagin, and A. N. Abiyaka, "Prospects For Use Of Finely Disperse Quartz Sands In Production Of Foam-Glass Crystalline Materials," *Glass and Ceramics,* vol. 65, pp. 319-321, Sep-Oct 2008.

[30] O. V. Kaz'mina, V. I. Vereshchagin, and A. N. Abiyaka, "Assessment of the compositions and components for obtaining foam-glass-crystalline materials from aluminosilicate initial materials," *Glass and Ceramics,* vol. 66, pp. 82-85, Mar 2009.

[31] J. Garcia-Ten, A. Saburit, M. J. Orts, E. Bernardo, and P. Colombo, "Glass foams from oxidation/reduction reactions using SiC, Si3N4 and AlN powders," *Glass Technology-European Journal of Glass Science and Technology Part A,* vol. 52, pp. 103-110, Aug 2011.

[32] A. S. Llaudis, M. J. O. Tari, F. J. G. Ten, E. Bernardo, and P. Colombo, "Foaming of flat glass cullet using Si3N4 and MnO2 powders," *Ceramics International,* vol. 35, pp. 1953-1959, Jul 2009.

[33] M. S. Garkavi, O. K. Mel'chaeva, and A. I. Nazarova, "Effect Of The Process Parameters Of Mix Preparation On The Properties Of Foam Glass," *Glass and Ceramics,* vol. 68, pp. 44-46, May 2011.

[34] N. Karsu, S. Yüksel, and M. Güden, "Foaming behavior of Ti6Al4V particle-added aluminum powder compacts," *Journal of Materials Science,* vol. 44, pp. 1494-1505, 2009.

[35] N. P. Bansal and R. H. Doremus, *Handbook of glass properties*, 1986.

[36] R. M. Silverstein, F. X. Webster, and D. J. Kiemle, *Spectrometric identification of organic compounds*: John Wiley & Sons, 2005.

[37] W. A. K. McCutcheon, P. L.; Lee, R. J.; Ramsey, M. S., "Understanding the Composition and Thermal History of Silicic Glasses Through Thermal Infrared Spectroscopy," 2012, p. 2543.

[38] M. Dussauze, V. Rodriguez, A. Lipovskii, M. Petrov, C. Smith, K. Richardson, T. Cardinal, E. Fargin, and E. I. Kamitsos, "How Does Thermal Poling Affect the Structure of Soda-Lime Glass?," *The Journal of Physical Chemistry C*, vol. 114, pp. 12754-12759, 2010/07/29 2010.

[39] D. V. Solomon, SE), Rossetti, Michael (Woburn, MA), "Foamed glass manufacture," United States Patent, 1996.

[40] G. S. G. Brusatin, L. Zampieri, P. Colombo, "Foam Glass form Cullet," *Glass Machinery & Accessories,* vol. 1, 2002.

[41] J. Quanli, Z. Haijun, L. Suping, and J. Xiaolin, "Effect of particle size on oxidation of silicon carbide powders," *Ceramics International,* vol. 33, pp. 309-313, 2007.

[42] E. Kreidl. Foam Glass [Online].

[43] (May, 2012). *Foam Glass*. Available: http://www.glazette.com/Glass-Knowledge-Bank-96/Foam-Glass.html

[44] A. Haibel, A. Rack, and J. Banhart, "Why are metal foams stable?," *Applied Physics Letters,* vol. 89, pp. 154102-3, 2006.

[45] D. Tulyaganov, H. Fernandes, S. Agathopoulos, and J. Ferreira, "Preparation and characterization of high compressive strength foams from sheet glass," *Journal of Porous Materials,* vol. 13, pp. 133-139, 2006.